LEVEL II

B.S. II

NUMERICAL STUDIES OF CONVERSION AND TRANSFORMATION IN A SURVEILLANCE SYSTEM EMPLOYING A MULTITUDE OF RADARS - PART II

R. G. Mulholland
D. W. Stout

DDC
JUL 30 1979

APRIL 1979
NAFEC REPORT

79 07 30 039

Prepared for

U.S. DEPARTMENT OF TRANSPORTATION
FEDERAL AVIATION ADMINISTRATION

NATIONAL AVIATION FACILITIES EXPERIMENTAL CENTER
Atlantic City, New Jersey 08405

1. Report No.	2. Government Accession No.	3. Recipient's Catalog No.
FAA-NA-79-18		

4. Title and Subtitle	5. Report Date
NUMERICAL STUDIES OF CONVERSION AND TRANSFORMATION IN A SURVEILLANCE SYSTEM EMPLOYING A MULTITUDE OF RADARS. PART II	Apr 79
	6. Performing Organization Code
	ANA-220

7. Author(s)	8. Performing Organization Report No.
R. G. Mulholland and D. W. Stout	FAA-NA-79-18

A072085

9. Performing Organization Name and Address	10. Work Unit No. (TRAIS)
Federal Aviation Administration National Aviation Facilities Experimental Center, Atlantic City, New Jersey 08405	
	11. Contract or Grant No.
	975-200-10A

12. Sponsoring Agency Name and Address	13. Type of Report and Period Covered
Federal Aviation Administration National Aviation Facilities Experimental Center, Atlantic City, New Jersey 08405	NAFEC
	14. Sponsoring Agency Code
	ANA-1

15. Supplementary Notes

58 p.

16. Abstract

Scale magnification and transformation errors are considered in the application of stereographic projection to the planar representation of target latitude and longitude relative to the reference ellipsoid in a multiple radar surveillance system. The representation is accomplished by a two-stage procedure. First, there is a conversion of target altitude together with target azimuth and slant range relative to a radar into a point on a plane unique to the radar. This is followed by a transformation that carries points on the local radar plane into points on a single master plane. Transformation error is viewed as the separation of images on the master plane of the same point in the local radar plane under an ideal mapping formula and polynomial approximations thereof. Tight upper and lower bounds are derived for the errors generated by these approximations under parameter constraints consistent with the structure of practical coverage regions. The transformation process is intimately connected with the factor by which the length of an infinitesimal arc on the reference ellipsoid is magnified under sterographic projection on the master plane. Minimax procedures for maintaining this magnification factor close to unity are considered. These procedures provide an upper bound on the deviation of the magnification factor from unity over the coverage region that is dependent on coverage region size.

17. Key Words	18. Distribution Statement
Multiple Radar Surveillance System Transformation Stereographic Projection Scale Magnification	Document is available to the U.S. public through National Technical Information Service, Springfield, Va. 22161

19. Security Classif. (of this report)	20. Security Classif. (of this page)	21. No. of Pages	22. Price
Unclassified	Unclassified	57	

Form DOT F 1700.7 (8-72)   Reproduction of completed page authorized

240550   79 07 30 039

METRIC CONVERSION FACTORS

Approximate Conversions to Metric Measures

Symbol	When You Know	Multiply by	To Find	Symbol
LENGTH				
in	inches	*2.5	centimeters	cm
ft	feet	30	centimeters	cm
yd	yards	0.9	meters	m
mi	miles	1.6	kilometers	km
AREA				
in²	square inches	6.5	square centimeters	cm²
ft²	square feet	0.09	square meters	m²
yd²	square yards	0.8	square meters	m²
mi²	square miles	2.6	square kilometers	km²
	acres	0.4	hectares	ha
MASS (weight)				
oz	ounces	28	grams	g
lb	pounds	0.45	kilograms	kg
	short tons (2000 lb)	0.9	tonnes	t
VOLUME				
tsp	teaspoons	5	milliliters	ml
Tbsp	tablespoons	15	milliliters	ml
fl oz	fluid ounces	30	milliliters	ml
c	cups	0.24	liters	l
pt	pints	0.47	liters	l
qt	quarts	0.95	liters	l
gal	gallons	3.8	liters	l
ft³	cubic feet	0.03	cubic meters	m³
yd³	cubic yards	0.76	cubic meters	m³
TEMPERATURE (exact)				
°F	Fahrenheit temperature	5/9 (after subtracting 32)	Celsius temperature	°C

*1 in = 2.54 (exactly). For other exact conversions and more detailed tables, see NBS Misc. Publ. 286, Units of Weights and Measures. Price $2.25, SD Catalog No. C13.10:286.

Approximate Conversions from Metric Measures
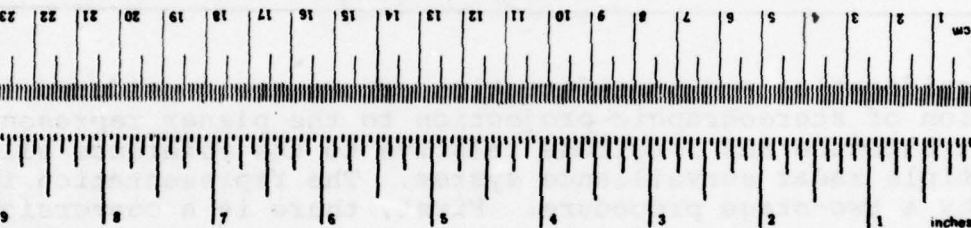
Symbol	When You Know	Multiply by	To Find	Symbol
LENGTH				
mm	millimeters	0.04	inches	in
cm	centimeters	0.4	inches	in
m	meters	3.3	feet	ft
m	meters	1.1	yards	yd
km	kilometers	0.6	miles	mi
AREA				
cm²	square centimeters	0.16	square inches	in²
m²	square meters	1.2	square yards	yd²
km²	square kilometers	0.4	square miles	mi²
ha	hectares (10,000 m²)	2.5	acres	
MASS (weight)				
g	grams	0.035	ounces	oz
kg	kilograms	2.2	pounds	lb
t	tonnes (1000 kg)	1.1	short tons	
VOLUME				
ml	milliliters	0.03	fluid ounces	fl oz
l	liters	2.1	pints	pt
l	liters	1.06	quarts	qt
l	liters	0.26	gallons	gal
m³	cubic meters	35	cubic feet	ft³
m³	cubic meters	1.3	cubic yards	yd³
TEMPERATURE (exact)				
°C	Celsius temperature	9/5 (then add 32)	Fahrenheit temperature	°F
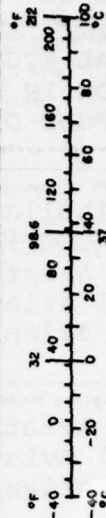
PREFACE

Acknowledgment is given to R. E. Lefferts who suggested the topic of this report. A great deal of benefit was derived from many conversations with him on the subject of multiple radar data processing systems. F. R. Mullin was also available for discussion. His extensive experience with the National Airspace System was a valuable source of information.

79 07 30 039

TABLE OF CONTENTS

LIST OF ILLUSTRATIONS

EXECUTIVE SUMMARY

This two-part paper is concerned with the application of stereographic projection to long-range surveillance systems employing a multitude of radars. It is an extension of earlier investigations of the same subject in connection with the Semi-Automatic Ground Environment System (SAGE) and the National Airspace System (NAS). Reconsideration of the topic at this time is appropriate in view of current trends in the air traffic control (ATC) community. Among these are improved accuracy of modern sensors now being contemplated as replacements for present operational radars, and the necessity of providing reliable forecasts of target position over long time intervals in advanced ATC functions such as Conflict Alert. A fundamental consideration is whether errors introduced by system implementation of stereographic projection are compatible with the quality of data offered by new radar technology and the objectives of advanced ATC services. Accordingly, this paper deals with the origin of such errors, the size of the errors, and alternative methods of controlling the errors in the context of the reference ellipsoid, a mathematical representation of the equipotential surface of the gravity field at mean sea level.

In long-range surveillance systems, target positions are represented by points in a so-called master plane. These points are obtained by mapping target altitude, azimuth, and slant range into the master plane. If the mapping is equivalent to stereographic projection of target latitude and longitude into the plane, then the master plane representation of a target is invariant to the radar from which azimuth and slant range are measured (provided, of course, that there is no measurement error). In a strict theoretical sense, it is possible to achieve such an equivalence by means of a two-stage procedure. First, there is a conversion of target altitude together with target azimuth and slant range relative to any given radar site into a point on a plane unique to the radar. This is followed by a transformation that carries points in the local radar plane into points on the master plane. In practice, exact duplication of ideal conversion and transformation processes is not possible. As a result, there are conversion errors and transformation errors, and these adversely affect the master plane representation of targets.

Part I of the paper treats conversion error; i.e., the distance between images in the local radar plane of target position (in terms of altitude, azimuth, and slant range) under ideal conversion and system implementations thereof. These images are viewed as elements of a complex plane in which the center of

coordinates represents the radar site. Thus, conversion error
can be expressed in terms of a range error equal to the
difference in moduli of two complex numbers and an angle error
equivalent to the difference between the arguments of the same
numbers. As the image of target position under ideal conversion
traverses a circle centered on the origin of coordinates, both
the angle error and the range error oscillate about median
values. The amplitude of each oscillation increases with the
radius of the circle. In addition, the median range error is
strongly dependent upon the radius of the circle. On the other
hand, the median angle error is identically zero.

In the case where error control is effected by commonly accepted
procedures, the angle error is less than $.0056°$ under standard
operational conditions. Moreover, the amplitude of the range
error is upper bounded by .02 nautical mile, whereas the median
range error can exceed .2 nautical mile. However, at least
from the theoretical point of view, there is another method of
error control capable of substantially eliminating the median
range error without disturbing the amplitudes of the angle and
range error oscillations. Needless to say, the reduction in
error attainable with the alternative method is significant.
While the practicality of the approach in the present environ-
ment is a moot question, the method does offer some interesting
possibilities in the context of a future replacement for the
NAS computer system.

Part II of the paper deals with transformation error; i.e., the
distance between images in the master plane of the same element
in the local radar plane under ideal transformation and poly-
nomial approximations thereof. Tight upper and lower bounds
are derived for the error generated by the nth order approxi-
mation to the ideal transformation equation under parameter
constraints consistent with the size of coverage areas
associated with current Air Traffic Control Centers (ARTCCs)
and the range of operational radars. In the case of
the first order approximation, the error can exceed .8 nautical
mile, whereas the error involved in the second order approxi-
mation is less than 8 meters. Clearly, from the standpoint of
error control, the first order approximation is far less
desirable than the second order approximation. However, the
error introduced by the nth order approximation is dependent
upon the location of the radar site from which positional
information is collected as well as the distance between the
target and the radar. Thus, as in the current ATC environment,
by using both approximations, it is possible to take advantage
of the simplicity of the first order approximation without
accepting an intolerable transformation error.

Although not altogether obvious, the transformation process is
intimately connected with the so-called magnification factor.
This is just the amount by which the length of an infinitesimal
arc on the reference ellipsoid is amplified under stereographic
projection into the master plane. The factor varies with the
position of the arc on the reference ellipsoid. For purposes of
convenience, as well as prediction accuracy, it is desirable
that the magnification factor be close to unity over the
coverage region of the surveillance system. In Part II,
practical procedures for accomplishing this desideratum
(other than those in current use) are discussed. These pro-
cedures provide an upper bound on the deviation of the
magnification factor from unity over the coverage region. The
bound is dependent on coverage region size. For example, if
the maximum distance between any two points in a coverage
region is on the order of 1,100 nautical miles, then it is
possible to keep the deviation below .004. As a result, the
magnification factor must fall between .996 and 1.004 over
the entire coverage region. In the case of coverage regions
with diameters less than 1,100 nautical miles, smaller bounds
on the deviation from unity are attainable.

In conclusion, it is emphasized that this investigation has been
conducted under the assumption that sensor measurements are
exact and data processing is carried out with infinite pre-
cision. In practice, this is not the case. Receiver front-end
noise exists, range and azimuth measurements are quantized
before being passed on to the central processor, trigonometric
functions and other standard mathematical relationships are
approximated in various ways by system hardware and software,
and multiplication and addition are carried out using finite
precision arithmetic. All of these contribute to error, and we
have no reason to believe the effect upon conversion and trans-
formation is inconsequential. In this sense, the results of
the paper should be viewed as representative of these processes
under ideal operating conditions.

1. Introduction

This is the second part of a two-part paper dealing with two-
dimensional representations of target position from measurements
of altitude, slant range, and azimuth in a multiple radar data
processing system. It is concerned with the case in which
such representations are realized by means of stereographic
projection. Assuming that the mean sea level surface of the
earth is an ellipsoid of revolution, this technique can be
used to establish a unique relationship between points on a
plane and orthogonal projections of points in space onto the
earth's surface. The latter can be determined from measure-
ments of slant range, azimuth, and altitude above mean sea
level. Thus, in the case of targets at the same latitude and
longitude but different altitudes, such measurements are
mapped into a single point on the plane. In this way, data
obtained from many radars can be used to assemble a single
planar representation of positions of aircraft and other
targets in three-dimensional space.

The mapping of target positions onto a single plane can be
viewed as a two-stage procedure. First, there is a conver-
sion of target altitude together with target slant range and
azimuth relative to any given radar site into a point on a
local radar plane. This is followed by a transformation
that carries points in the local plane into points on a
single master plane. Thus, there are as many local planes as
there are radars, and each of these is mapped into the master
plane to establish the final planar representation of positions
of targets within the coverage region of the overall sur-
veillance system.

Ideally, conversion involves a determination of the ortho-
gonal projection of target position on the ellipsoidal

1

representation of the mean sea level surface of the earth, a mapping of the projection onto a so-called conformal sphere, and stereographic projection of the spherical surface onto the local radar plane. Transformation, in the ideal sense, is realized by a bilinear transformation that takes the local plane into the master plane. When carried out in this fashion, the process of conversion and transformation is equivalent to the three steps of conversion alone with the exception that the local and master planes are the same. Thus, under ideal conversion and transformation, the planar representation of a target is invariant to the radar with respect to which slant range and azimuth are measured.

In practice, it is difficult to realize the ideal forms of conversion and transformation. As a result, modifications of these procedures are encountered in operational systems. Theoretical treatments of the subject can be found in [1], [2], [3], [4], and [5]. Numerical studies of conversion are reported in Part I [6] of the current paper. In this part of the paper; i.e., Part II, the transformation process is examined. Objectives of this investigation are to assemble a comprehensive picture of pertinent theoretical results applicable to the transformation process, to provide numerical results characterizing differences between ideal procedures and those encountered in practice, to consider alternative methods for controlling master plane magnification of distance on an ellipsoidal representation of the mean sea level surface of the earth, and to examine the increment in master plane representation of target location due to an increment in position on the local radar plane.

The next section summarizes essential features of geodetic coordinates used in future developments. Section 3 reviews the relationship between conformal and geodetic

2

latitudes as well as the mathematical expressions by which the surface of a conformal sphere can be stereographically projected onto a tangent plane. Section 4 is concerned with the connection between stereographic projection, the transformation equation, and the planar representation of targets in multiple radar surveillance systems. Section 5 treats the factor by which distance on an ellipsoidal earth model is magnified in the master plane. In addition, consideration is given to the minimization of the maximum deviation of this factor from unity by an appropriate selection of the radius for the conformal sphere that supports the master plane. Minimax solutions for the special case of circular coverage regions are discussed in Section 6. Section 7 deals with constraints on parameters that are consistent with the size of coverage regions in current long-range air traffic control surveillance systems. Differences between the transformation equation and polynomial approximations thereof employed in some operational systems are discussed in Section 8. Section 9 provides numerical results that characterize these differences under the constraints of Section 7 when control of the magnification factor is effected by means of the minimax criteria outlined in Section 5. The effect of an increment in position in the local radar plane on the transformation process is described in Section 10. Concluding remarks appear in Section 11.

2. Reference Ellipsoid

The gravity field of the earth is the result of two forces--
the centrifugal force due to the earth's rotation and the
force of mass attraction between the earth and other bodies.
It can be described in terms of equipotential surfaces, and
the force of gravity is perpendicular to such surfaces. The
equipotential surface at mean sea level is called the geoid.
It is irregular and hence unsuitable as a basis for a coor-
dinate system. The geoid can be closely approximated by an
ellipsoid of revolution called the reference ellipsoid, and
this is often used for purposes of navigation, gravity
computations, etc.

An ellipsoid is illustrated in Figure 1. It has a semi-
major axis of length a (the equitorial radius) and a
semi-minor axis of length b (the polar radius). In the case
of the reference ellipsoid [7],

$$a = 6,378,388 \text{ meters}$$
$$b = 6,356,912 \text{ meters.}$$

The direction of the earth's rotation is indicated by the
arrowhead (pointing north) on the minor axis in conjunction
with the usual right-hand rule. The ellipsoid is split
into halves by a plane (the equatorial plane) perpendicular
to the minor axis. These correspond to the usual notions
of Northern and Southern Hemispheres. Planes parallel to
the equatorial plane cut the ellipsoid in circles called
parallels. Planes containing the minor or polar axis cut it
in ellipses. The portion of any such ellipse on either
side of the polar axis is called a meridian.

A point Q on the surface of the ellipsoid is specified by
its geodetic coordinates in terms of meridians and parallels.
Except in the case of the North or South Pole, the point is

4

the intersection of only one meridian and one parallel. In the case where it is a pole, the corresponding parallel is a point and so there is no ambiguity.

Meridians and parallels are usually expressed as angles, namely, latitude and longitude. These can be defined in terms of a Cartesian system with origin at the center of the ellipsoid. Referring to Figure 1, this system consists of the polar axis and two orthogonal axes in the equatorial plane. Positive directions along the axes are indicated by unit vectors $\hat{i}$, $\hat{j}$, and $\hat{k}$. The meridian passing through Q is described by the angle λ (longitude) measured in the equatorial plane counter to the direction of the earth's rotation between the plane containing the arrows marked $\hat{j}$ and $\hat{k}$ and that containing Q and the polar axis. The corresponding parallel is defined by the angle L (latitude) in the latter plane measured from the equatorial plane to the line perpendicular to the ellipsoid at Q. When Q is in the Northern Hemisphere, L is nonnegative and does not exceed 90°. Otherwise, it is negative, but not less than -90°.

As indicated in Figure 1, the position vector $\bar{s}(L,\lambda)$ of Q can be represented by an arrow drawn from the center of the ellipsoid to Q. It can be shown that

$$\bar{s}(L,\lambda) = \frac{a}{\sqrt{1-e^2\sin^2 L}} [\cos L \, (\sin\lambda \, \hat{i} + \cos\lambda \, \hat{j}) + (1-e^2) \sin L \, \hat{k}] \quad (1)$$

where e is the ellipticity of the ellipsoid; i.e.,

$$e^2 = a^{-2}(a^2 - b^2). \quad (2)$$

5

The unit outward normal $\hat{u}_3(L,\lambda)$ to the ellipsoid at Q can be expressed as

$$\hat{u}_3(L,\lambda) = \cos L \ (\sin\lambda\hat{i}+\cos\lambda\hat{j})+\sin L \ \hat{k} \tag{3}$$

Thus, the position vector of a point target P at altitude H above Q is just the sum of the position vector of Q and the product of H and $\hat{u}_3(L,\lambda)$.

In later sections, we shall find it convenient to refer to orthogonal unit vectors $\hat{u}_1(L,\lambda)$ and $\hat{u}_2(L,\lambda)$. In Figure 1, these are pictured as lying in the plane tangent to the ellipsoid at Q. In addition, $\hat{u}_2(L,\lambda)$ lies in the plane defined by the λ-meridian and is directed from the South to North Pole. In can be expressed as

$$\hat{u}_2(L,\lambda)=-\sin L \ (\sin\lambda\hat{i}+\cos\lambda\hat{j})+\cos L \ \hat{k} \tag{4}$$

The remaining vector can be viewed as an arrow in the plane defined by the L-parallel pointing in the direction of the earth's rotation. It can be written as the cross product

$$\hat{u}_1(L,\lambda)=\hat{u}_2(L,\lambda)\times\hat{u}_3(L,\lambda)=-\cos\lambda\hat{i}+\sin\lambda\hat{j} \tag{5}$$

In the degenerate case where Q is either the North or South Pole, it is sufficient to consider $\hat{u}_1(L,\lambda)$ and $\hat{u}_2(L,\lambda)$ to be any orthogonal pair of unit vectors in the tangent plane such that $\hat{u}_1(L,\lambda)\times\hat{u}_2(L,\lambda)$ is equivalent to $\hat{u}_3(L,\lambda)$.

6

FIGURE 1. REFERENCE ELLIPSOID

3. Conformal Spheres and Stereographic Projection

For our purposes, any sphere with center colocated with the center of the ellipsoid of Figure 1 is a conformal sphere. Since an ellipsoid is itself a sphere when the lengths of the major and minor axes are the same, we can talk about points on a conformal sphere in terms of latitude and longitude in the same way we use these angles to describe points on the ellipsoid. With this understanding, we are in a position to discuss mappings that send points on the ellipsoid into points on a conformal sphere. One such mapping, which we denote by

$$F: (L, \lambda) \to (\emptyset, \lambda), \tag{6}$$

sends the point Q with geodetic coordinates (L, λ) on the ellipsoid into the point $(\emptyset, \lambda)$ on a conformal sphere via the relationship

$$\left[\frac{1-e \sin L}{1+e \sin L}\right]^{\frac{e}{2}} \tan\left[\frac{\pi}{4}+\frac{L}{2}\right] = \tan\left[\frac{\pi}{4}+\frac{\emptyset}{2}\right] \tag{7}$$

The mapping is one to one. Moreover, Q and its image have the same longitude λ, but different latitudes. The latitude $\emptyset$ of the image is often referred to as the conformal latitude of Q to distinguish it from the geodetic latitude L.

As already pointed out, a sphere is a special case of an ellipsoid. Hence, the notation developed in the previous section is applicable to conformal spheres. Accordingly, as illustrated in Figure 2, $\hat{u}_3(\emptyset_s, \lambda_s)$ can be viewed as a unit vector normal to the surface of a conformal sphere at longitude λ_s and conformal latitude $\emptyset_s$. Likewise, $\hat{u}_1(\emptyset_s, \lambda_s)$ and $\hat{u}_2(\emptyset_s, \lambda_s)$ can be represented as arrows lying in the plane tangent to the sphere at $(\emptyset_s, \lambda_s)$. Adopting the convention

8

that $\hat{u}_2(\emptyset_s, \lambda_s)$ indicates the direction of increasing imaginary parts of complex numbers, this representation defines a complex plane. In the following paragraphs, we will outline the method of stereographic projection as a mapping of the spherical surface onto this plane.

Referring to Figure 2, the line normal to the sphere at $(\emptyset_s, \lambda_s)$ passes through the center and intersects the spherical surface at $(-\emptyset_s, \lambda_s + \pi)$. The latter is the focal point for stereographic projection. Under the projection mapping, the image of a point A on the spherical shell is just the point I where the line through A and the focal point intersects the complex plane.

Suppose $\emptyset$ is the latitude and λ the longitude of A, and let x and y denote the real and imaginary parts of the complex representation of I. Then, assuming the radius of the sphere is E_s, it can be shown that stereographic projection is equivalent to the mapping [4]

$$G_s : (\emptyset, \lambda) \rightarrow x + iy \tag{8}$$

where

$$x = \frac{2E_s \cos \emptyset \sin (\lambda_s - \lambda)}{1 + \sin \emptyset_s \sin \emptyset + \cos \emptyset_s \cos \emptyset \cos (\lambda_s - \lambda)} \tag{9}$$

$$y = \frac{2E_s [\cos \emptyset_s \sin \emptyset - \sin \emptyset_s \cos \emptyset \cos (\lambda_s - \lambda)]}{1 + \sin \emptyset_s \sin \emptyset + \cos \emptyset_s \cos \emptyset \cos (\lambda_s - \lambda)} \tag{10}$$

and i is $\sqrt{-1}$. This is a one-to-one relation. The inverse mapping G_s^{-1} is defined by

$$\sin \emptyset = \frac{(4E_s^2 - x^2 - y^2) \sin \emptyset_s + 4E_s y \cos \emptyset_s}{4E_s^2 + x^2 + y^2} \tag{11}$$

9

$$\sin(\lambda - \lambda_s) = \frac{-4E_s x}{\sqrt{[-4E_s x]^2 + [(4E_s^2 - x^2 - y^2)\cos\phi_s - 4E_s\, y \sin\phi_s]^2}} \qquad (12)$$

$$\cos(\lambda - \lambda_s) = \frac{(4E_s^2 - x^2 - y^2)\cos\phi_s - 4E_s\, y \sin\phi_s}{\sqrt{[-4E_s x]^2 + [(4E_s^2 - x^2 - y^2)\cos\phi_s - 4E_s\, y \sin\phi_s]^2}} \qquad (13)$$

10

IMAGINARY AXIS

I

x

TANGENT PLANE

y

$\hat{u}_2 (\phi_s, \lambda_s)$

$\hat{u}_3 (\phi_s, \lambda_s)$

REAL AXIS

A

$\hat{u}_1 (\phi_s, \lambda_s)$

$\hat{k}$

$\hat{j}$

ϕ_s

λ_s

$\hat{i}$

$(-\phi_s, \pi + \lambda_s)$

CONFORMAL SPHERE
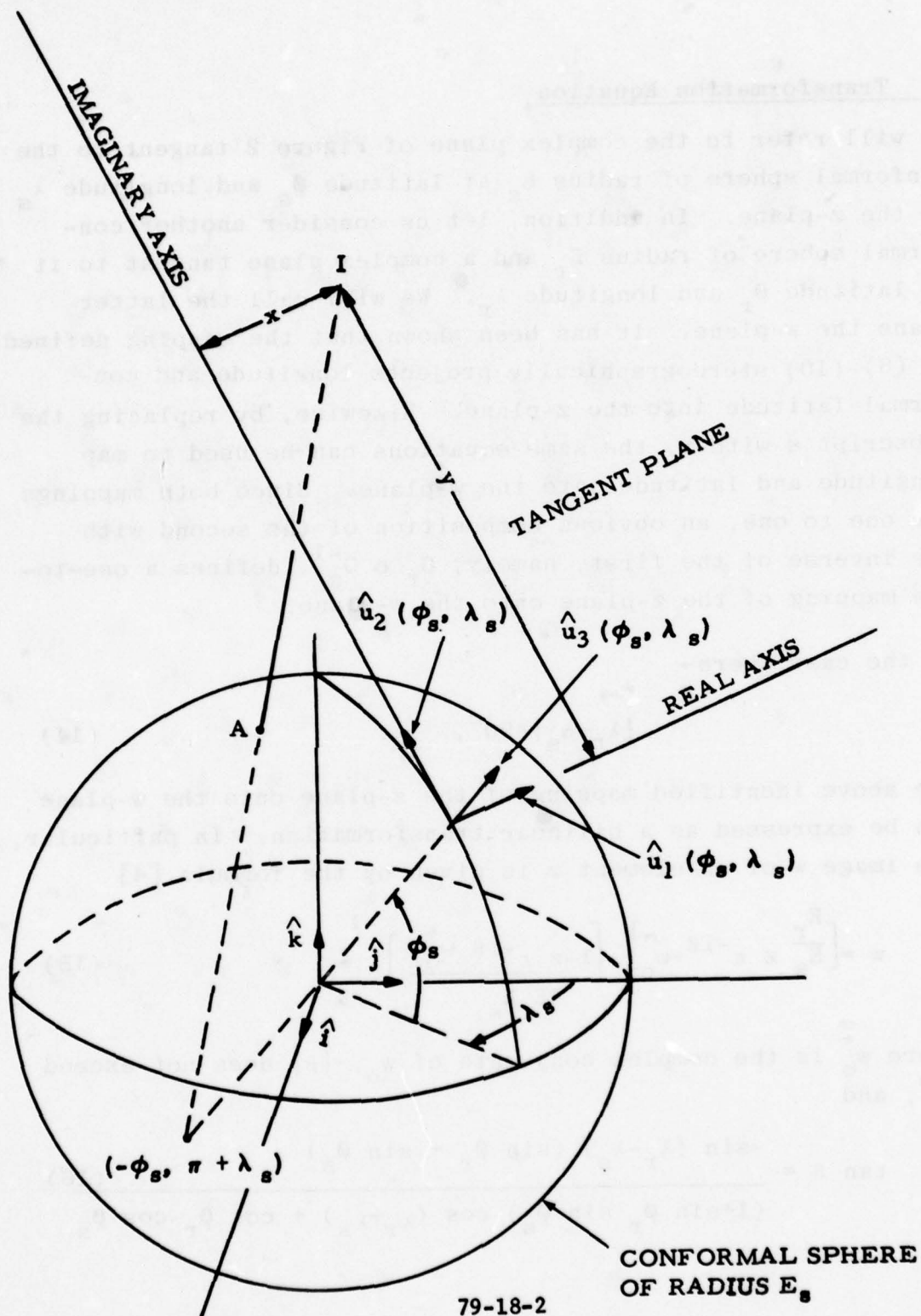OF RADIUS E_s

79-18-2

FIGURE 2.   STEREOGRAPHIC PROJECTION

11

4. Transformation Equation

We will refer to the complex plane of Figure 2 tangent to the conformal sphere of radius E_s at latitude ϕ_s and longitude λ_s as the z-plane. In addition, let us consider another conformal sphere of radius E_r and a complex plane tangent to it at latitude ϕ_r and longitude λ_r. We will call the latter plane the w-plane. It has been shown that the mapping defined by (8)-(10) stereographically projects longitude and conformal latitude into the z-plane. Likewise, by replacing the subscript s with r, the same equations can be used to map longitude and latitude into the w-plane. Since both mappings are one to one, an obvious composition of the second with the inverse of the first, namely, $G_r \circ G_s^{-1}$, defines a one-to-one mapping of the z-plane onto the w-plane.

In the case where

$$|\lambda_r - \lambda_s| < 90^{\circ}, \tag{14}$$

the above identified mapping of the z-plane onto the w-plane can be expressed as a bilinear transformation. In particular, the image w of an element z is given by the formula [4]

$$w = \left[\frac{E_r}{E_s} z \, \varepsilon^{-i\beta} + w_o \right] \left[1 - \frac{z \, \varepsilon^{-i\beta} \, w_o^*}{4 E_r E_s} \right]^{-1}. \tag{15}$$

where w_o^* is the complex conjugate of w_o, $|\beta|$ does not exceed 90°, and

$$\tan \beta = \frac{-\sin(\lambda_r - \lambda_s)(\sin\phi_r + \sin\phi_s)}{(1 + \sin\phi_r \sin\phi_s)\cos(\lambda_r - \lambda_s) + \cos\phi_r \cos\phi_s} \tag{16}$$

12

Obviously, the complex number w_o is just the image of the origin of the z-plane. However, it is clear from the definition of the mapping that any element of the z-plane and its image represent the same latitude and longitude. Consequently, the real and imaginary parts of w_o can be found from (9) and (10) by replacing the subscript s with r. As will be seen shortly, the constraint (14) is not difficult to meet in many practical situations.

Equation (15) is important in some applications where measurements taken from a multitude of far-flung radars are used for surveillance purposes at a single site, such as an air route traffic control center. Estimates of target longitude and conformal latitude from measurements of slant range and azimuth by a single radar in conjunction with reports of target altitude can be formed by means of a mapping into a complex plane tangent to an appropriate sphere at the longitude and conformal latitude of the radar site. This plane corresponds to the z-plane, and the radius E_s of the sphere is the radius of the earth $|\bar{s}(L_s, \lambda_s)|$ at the longitude λ_s and geodetic latitude L_s of the radar [6]. There are as many such complex planes as there are radars. Each of these is mapped into a single master plane, corresponding to the w-plane, via a functional relationship analogous to (15). Thus, images on the master plane represent longitude and conformal latitude of targets within the composite of the coverage regions of many individual radars. Clearly, the constraint (14) will be satisfied so long as the absolute difference between the longitudes of the points of tangency of the master plane and the local radar plane does not exceed 90° for every radar.

13

5. Magnification Factor

Consider a target at longitude λ and geodetic latitude L. Let $\emptyset$ be the corresponding conformal latitude of the target. Then, $(\emptyset, \lambda)$ is the image of (L, λ) under the mapping F defined by (6) and (7). Also, let w represent the w-plane image of $(\emptyset, \lambda)$ under the projection mapping G_r defined by (8)-(10) with subscript s replaced by r. Ideally, both L and λ can be determined from target slant range, azimuth, and altitude above the reference ellipsoid. Thus, the mapping

$$M = G_r \circ F \qquad (17)$$

sends (L, λ) into w, and it can be viewed as the mechanism by which target positions in the coverage region of a multiple radar surveillance system are carried into the master plane.

Under the mapping M, an infinitesimal arc of length ds_e at (L, λ) on the ellipsoid is carried into an infinitesimal arc of length ds_m on the master plane. The ratio ds_m/ds_e is called the magnification factor, and it can be expressed as [8], [9]

$$\frac{ds_m}{ds_e} = \frac{2E_r \cos \emptyset}{\dfrac{a \cos L}{\sqrt{1-e^2 \sin^2 L}}\, [1+\sin \emptyset \sin \emptyset_r + \cos \emptyset \cos \emptyset_r \cos (\lambda_r - \lambda)]} \qquad (18)$$

Thus, the magnification factor is dependent upon the radius E_r of the conformal sphere that supports the master plane, the point of support or tangency $(\emptyset_r, \lambda_r)$, and the position (L, λ) of the incremental arc of length ds_e on the ellipsoid.

Let C represent the set of all pairs (L, λ) in the coverage region of the surveillance system. Also, let us suppose that the point of tangency $(\emptyset_r, \lambda_r)$ of the master plane has been selected; e.g., it might be any latitude-longitude pair for which $F^{-1} (\emptyset_r, \lambda_r)$ can be reasonably construed to be a central

14

point of the coverage region. Then, in order that the mapping M preserve distance, the radius E_r must be chosen so that the magnification factor is close to 1 for all (L,λ) in C. In the next few paragraphs, we will show how this can be accomplished in a minimax sense.

The angle $\Gamma(\emptyset,\lambda)$ between the position vectors of $(\emptyset,\lambda)$ and $(\emptyset_r,\lambda_r)$ on a conformal sphere is bounded below by 0° and above by 180°. The cosine of this angle is just the inner product of these vectors in the case of the sphere of unit radius, namely,

$$\cos \Gamma(\emptyset,\lambda) = \bar{s}(\emptyset,\lambda) \cdot \bar{s}(\emptyset_r,\lambda_r)$$

$$= \sin \emptyset \sin \emptyset_r + \cos \emptyset \cos \emptyset_r \cos (\lambda-\lambda_r) \tag{19}$$

Since $\emptyset$ can be regarded as the image of L under a one-to-one mapping f specified by (7), it is appropriate to define a function $k(\emptyset,\lambda)$ by

$$k(\emptyset,\lambda) = h(\emptyset) \ g(\emptyset,\lambda) \tag{20}$$

where

$$h(\emptyset) = \frac{\cos \emptyset \ \sqrt{1-e^2 \sin^2 f^{-1}(\emptyset)}}{\cos f^{-1}(\emptyset)} \tag{21}$$

$$g(\emptyset,\lambda) = 2[1+\cos \Gamma(\emptyset,\lambda)]^{-1}. \tag{22}$$

The magnification factor is just the product of this function and the ratio E_r/a. Thus, within the coverage region C, or equivalently, the region F(C), the maximum deviation of the magnification factor from 1 is given by

$$d(E_r) = \max\left[\left|\frac{E_r}{a} k_M-1\right|, \left|\frac{E_r}{a} k_m-1\right|\right] \tag{23}$$

15

where[1]

$$k_M = \max_{(\emptyset, \lambda) \in F(C)} k(\emptyset, \lambda) \tag{24}$$

$$k_m = \min_{(\emptyset, \lambda) \in F(C)} k(\emptyset, \lambda). \tag{25}$$

Consequently, any positive number E_r satisfying the relation

$$d(E_r) = \min_{x > 0} d(x) \tag{26}$$

can be viewed as a radius for the spherical support of the master plane that minimizes the maximum deviation.

Obviously, both k_m and k_M are positive, and the former cannot exceed the latter. Thus, from Figure 3, it is clear that there exists a positive number between a/k_m and a/k_M such that

$$\frac{E_r}{a} k_M - 1 = 1 - \frac{E_r}{a} k_m \geq 0, \tag{27}$$

namely,

$$E_r = \frac{2a}{k_M + k_m}. \tag{28}$$

Moreover, from the same figure, it is clear that (28) satisfies (26) and so must be a minimax solution for the radius of the spherical support for the master plane. The corresponding maximum deviation of the magnification factor from 1 is

$$d\left(\frac{2a}{k_M + k_m}\right) = \frac{k_M - k_m}{k_M + k_m}. \tag{29}$$

---

[1] We tacitly assume here that the coverage region C is closed and bounded in the topological sense to insure the existance of k_m and k_M. From a practical viewpoint, this is not a serious restriction.

16

In practice, it may be difficult to find k_M and k_m. On the
other hand, suppose $\Gamma(\phi,\lambda)$ is upper bounded by ξ_o on $F(C)$,
and let us consider the sets

$$X(\xi) = \{(\phi,\lambda):\Gamma(\phi,\lambda) = \xi\} \tag{30}$$

$$\bar{X}(\xi) = \{(\phi,\lambda):\Gamma(\phi,\lambda) \leq \xi\}. \tag{31}$$

The set $\bar{X}(\xi)$ can be viewed as a portion of the surface of a
conformal sphere having a circular boundary, namely, $X(\xi)$.
In fact, it can be viewed as a circular region with center
(ϕ_r,λ_r) and angular radius ξ. When ξ equals or exceeds ξ_o,
it contains $F(C)$ as a subset. Thus, the maximum value k_M
of $k(\phi,\lambda)$ on $F(C)$ cannot exceed the maximum k_M' of the same
function on $\bar{X}(\xi_o)$. Likewise, the minimum k_m' of $k(\phi,\lambda)$ on
$\bar{X}(\xi_o)$ cannot exceed the minimum k_m of the function on $F(C)$.
Consequently,

$$\frac{k_M'-k_m'}{k_M'+k_m'} - \frac{k_M-k_m}{k_M+k_m} = \frac{2(k_M'k_m-k_m'k_M)}{(k_M'+k_m')(k_M+k_m)} \geq 0. \tag{32}$$

In other words, the maximum deviation of the magnification
factor from 1 obtained from the minimax solution for the
circular region $\bar{X}(\xi_o)$ upper bounds the maximum deviation
obtained from the minimax solution for $F(C)$.

Obviously, the minimax solution for $\bar{X}(\xi_o)$ is not necessarily
optimal for the actual coverage region C, or its equivalent
$F(C)$. However, if the solution provides extreme values of the
magnification factor that are very close to 1, then this may
not be a serious consideration. We will deal with this matter
further in the next section in which k_M and k_m are evaluated
for the case where $F(C)$ is itself circular.

17
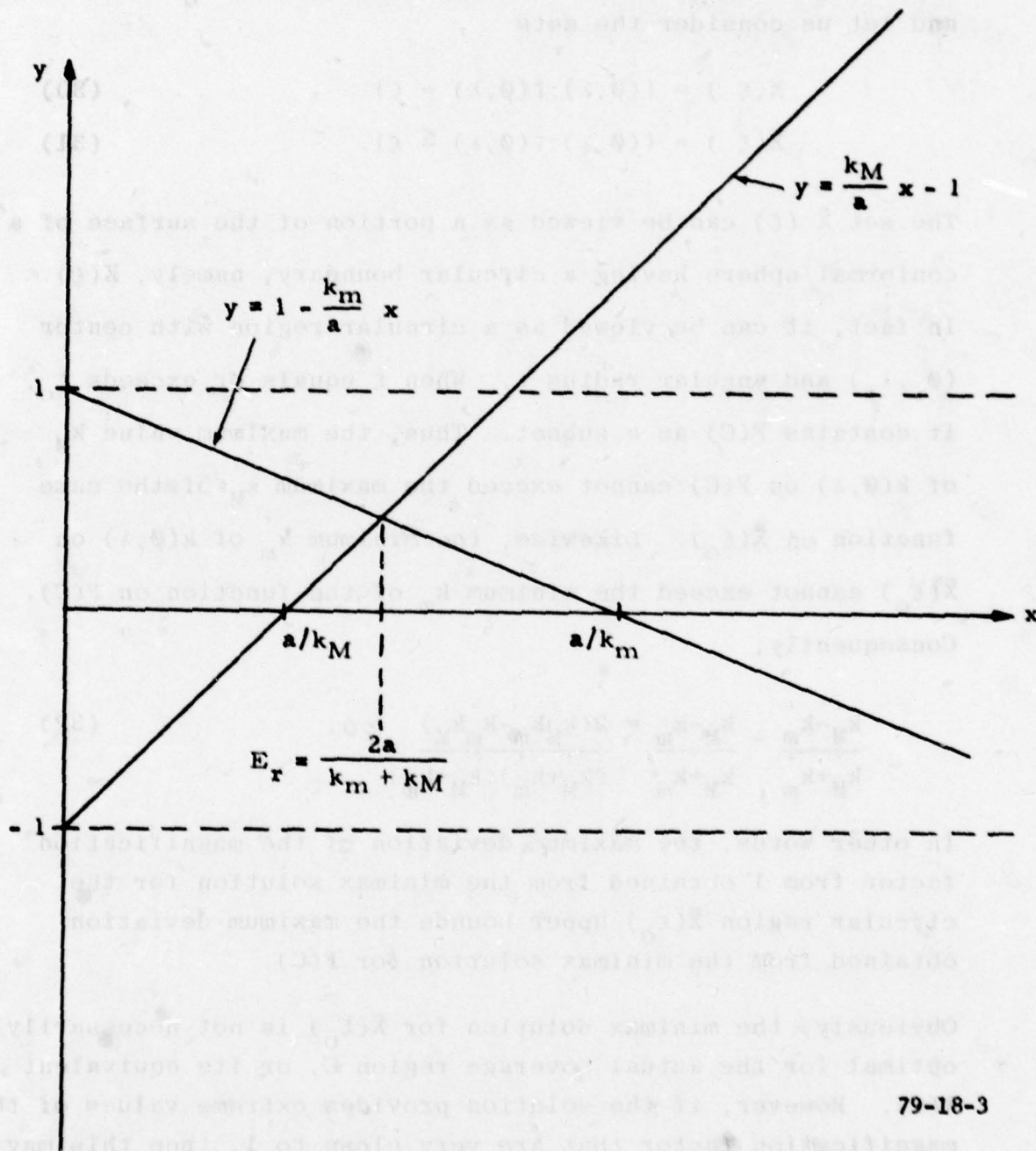
FIGURE 3.   MINIMAX SOLUTION FOR RADIUS OF SPHERICAL
SUPPORT OF MASTER PLAN

79-18-3

6. Magnification for Circular Geometries

The function $k(\phi,\lambda)$ is the product of $h(\phi)$ and $g(\phi,\lambda)$ defined by (21) and (22). Numerical investigations of $h(\phi)$ indicate it is a monotone function rising from 1 at 0° to a value less than 1.0034 at 90°. From (30), the angle $\Gamma(\phi,\lambda)$ assumes the constant value ξ on the set $X(\xi)$. As a result, $g(\phi,\lambda)$ is a constant on the same set. Thus, on $X(\xi)$, $k(\phi,\lambda)$ assumes its maximum (minimum) value at the point for which $|\phi|$ is maximum (minimum). This is located on the λ_r-meridian or the $(\pi+\lambda_r)$-meridian. For example, if ϕ is bounded below by 0° and above by 90° for all (ϕ,λ) in $X(\xi)$, then $k(\phi,\lambda)$ is greatest at $(\phi_r+\xi,\lambda_r)$ and least at $(\phi_r-\xi,\lambda_r)$.

As pointed out earlier, the angle $\Gamma(\phi,\lambda)$ necessarily lies in the interval bounded by 0° and 180°. Consequently, $g(\phi,\lambda)$ increases with increasing values of this angle. Thus, the constant value assumed by $g(\phi,\lambda)$ on the set $X(\xi)$ is a monotonic increasing function of ξ. As will be seen, this observation and those of the preceding paragraph are useful in the determination of k_M and k_m in the case where $F(C)$ is circular.

Suppose now that the coverage region C is such that its image under F is the circular region $\bar{X}(\xi_o)$. This region is just the union of all sets $X(\xi)$ for which

$$0 \leq \xi \leq \xi_o \tag{33}$$

In view of our earlier observations regarding the set $X(\xi)$, it is apparent that $k(\phi,\lambda)$ must assume its extreme values on $\bar{X}(\xi_o)$ somewhere in the intersection of the set with the union of the λ_r-meridian and the $(\pi+\lambda_r)$-meridian. As will be shown next, in the case of some circular regions, we can be more specific than this.

19

Consider the case where the latitude $\emptyset_r$ of the center of the circular region $\bar{X}(\xi_o)$ is not less than 0°, and $\emptyset_r+\xi_o$ does not exceed 90°. Since the constant value assumed by $g(\emptyset,\lambda)$ on $\bar{X}(\xi)$ increases monotonically with ξ, and $h(\emptyset)$ increases monotonically with increasing values of $|\emptyset|$, it is apparent that $k(\emptyset,\lambda)$ takes on its maximum value k_M in $\bar{X}(\xi_o)$ at $(\emptyset_r+\xi_o,\lambda_r)$. It is equally apparent that this function will assume its minimum value k_m somewhere on the λ_r-meridian between latitudes $\emptyset_r$ and $\emptyset_r-\xi_o$. In fact, we expect the function $k(\emptyset_r-\xi,\lambda_r)$ to decrease as ξ increases from 0°, achieve a minimum at some angle ξ' between 0° and $\emptyset_r$, and then continue to rise[2] until ξ reaches the value $\emptyset_r+90^o$. Consequently, k_m is invariant to the angular radius ξ_o of the circular set $\bar{X}(\xi_o)$ in the range bounded by ξ' and $90^o-\emptyset_r$, assuming, of course, that the latter exceeds the former.

As a concrete example, consider the case in which the latitude $\emptyset_r$ of the center of $\bar{X}(\xi_o)$ is 38°. Then, ξ' is 0.373^o and k_m is 1.00127 whenever

$$\xi' \leq \xi_o \leq 52^o. \tag{34}$$

Figure 4 illustrates the maximum value of k_M of $k(\emptyset,\lambda)$ on $\bar{X}(\xi_o)$ as a function of the angular radius ξ_o. Minimax solutions for the radius of the spherical support of the master plane are shown in Figure 5 for different latitudes of the center including the case where it is 38°. Corresponding values of the absolute difference between the magnification factor and 1 appear in Figure 6. The difference is not a monotone function of the latitude of the center of the circular region. For example, the differences realized with center latitudes 0° and 38° bound the difference for a center latitude of 70°.

---

[2] The expectation of a single minimum is supported by numerical results. Nevertheless, it is a matter of conjecture rather than proof.
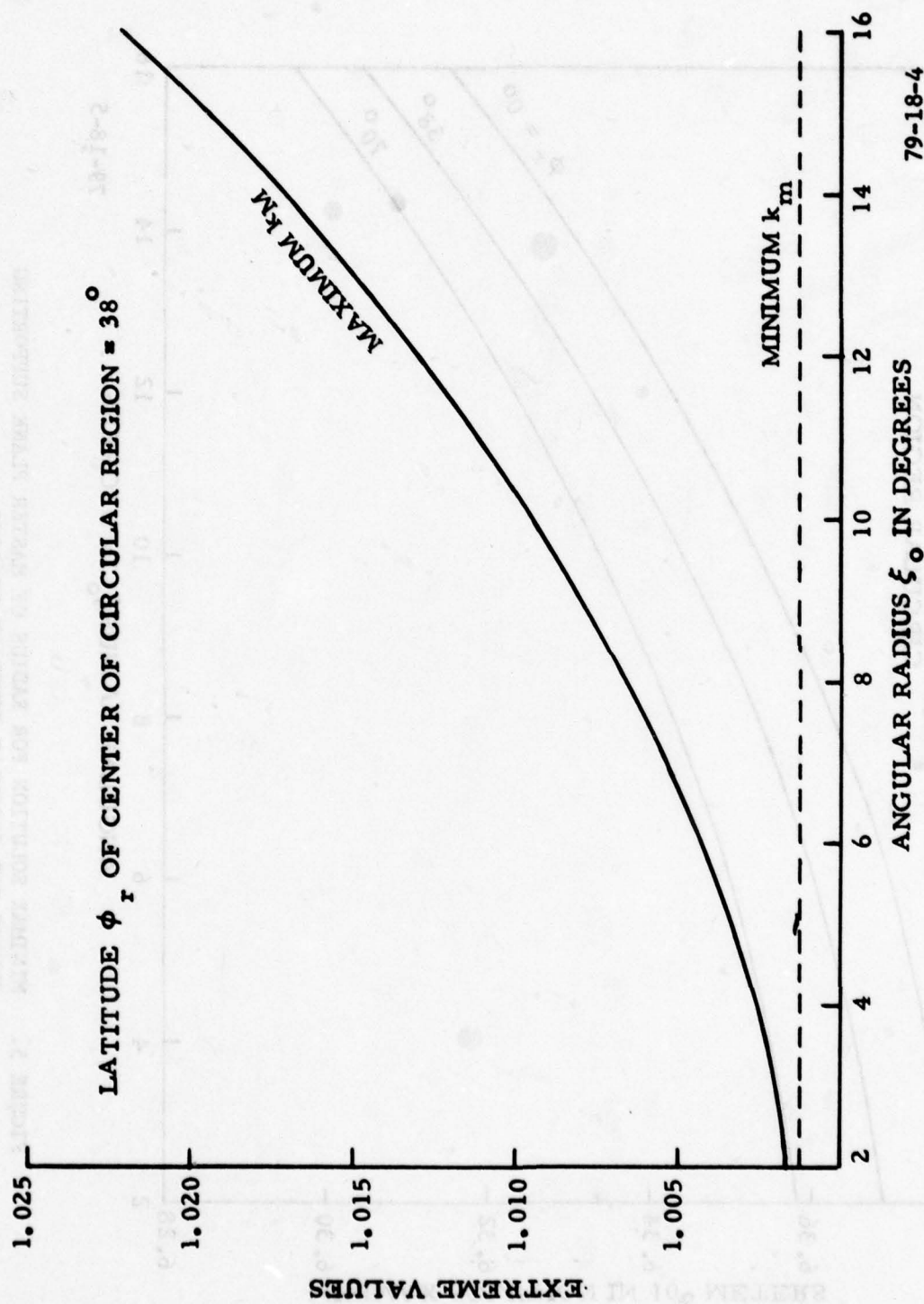
FIGURE 4.   EXTREME VALUES OF THE NORMALIZED MAGNIFICATION FACTOR ON A CIRCULAR REGION
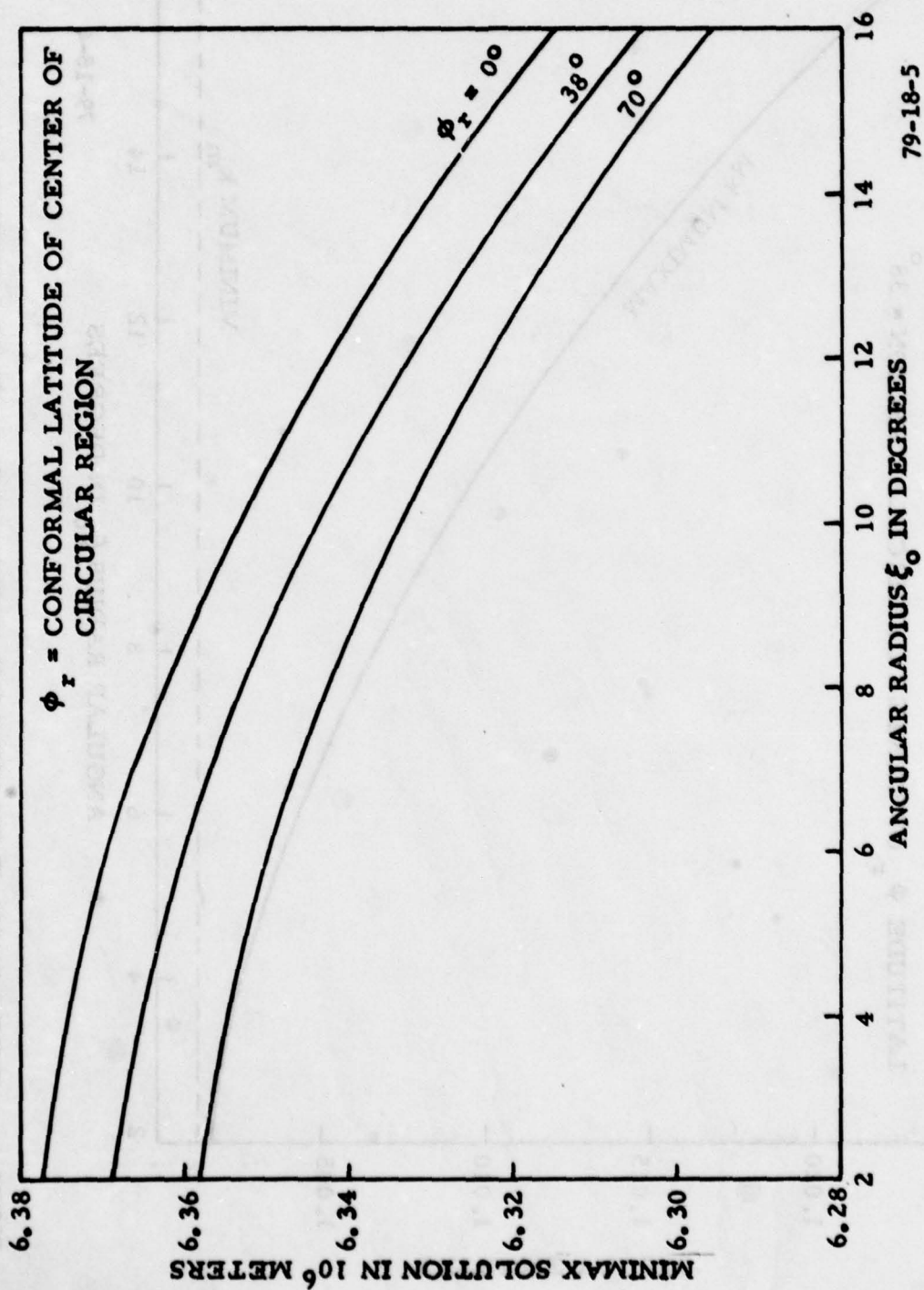
21

FIGURE 5.   MINIMAX SOLUTION FOR RADIUS OF MASTER PLANE SUPPORTING
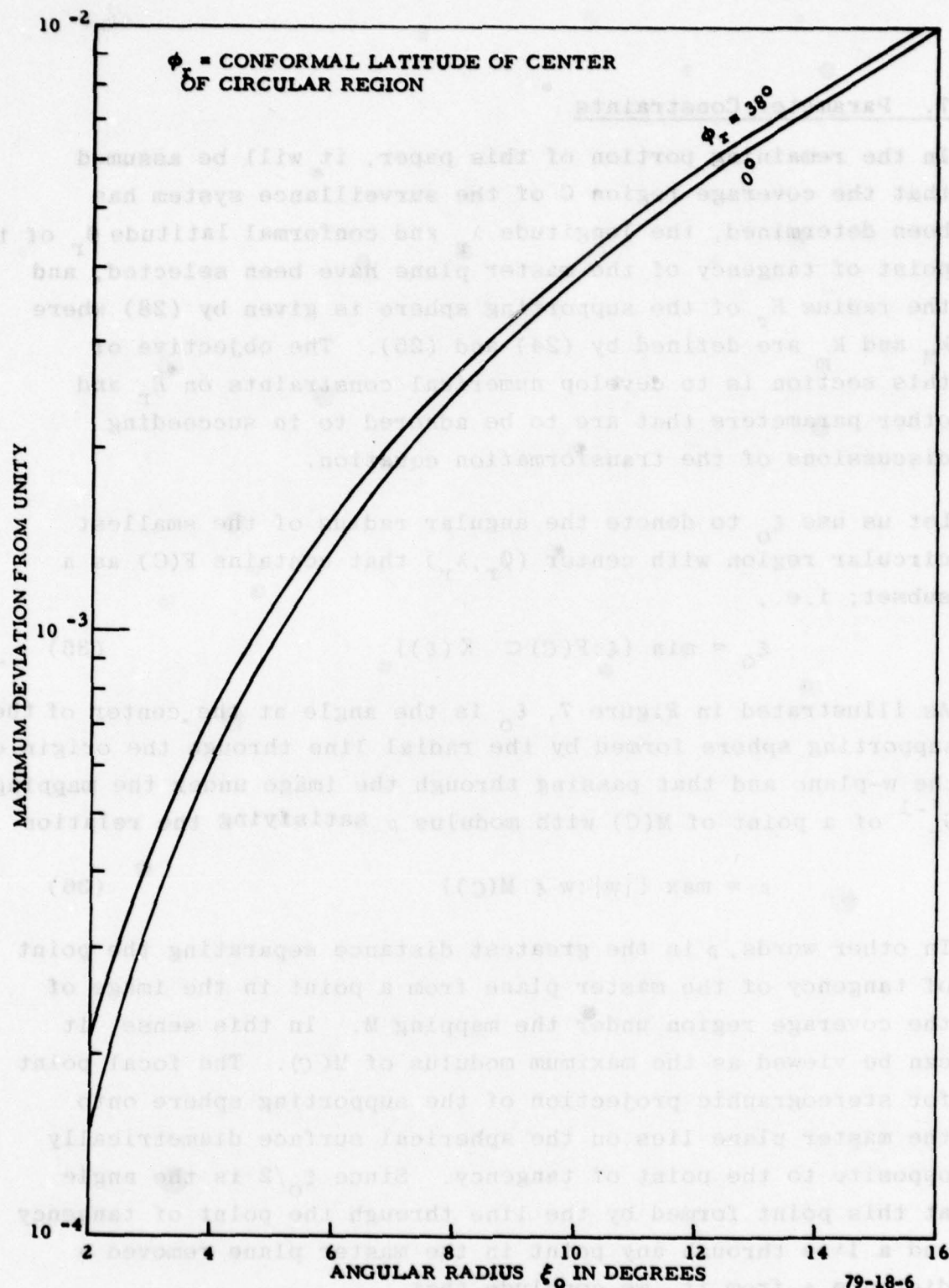SPHERE FOR CIRCULAR COVERAGE REGIONS

22

FIGURE 6.   MAXIMUM DEVIATION OF MAGNIFICATION FACTOR FROM UNITY OVER
CIRCULAR REGIONS CORRESPONDING TO MINIMAX SOLUTIONS FOR
THE SPHERICAL SUPPORT OF THE MASTER PLANE

23

7. Parameter Constraints

In the remaining portion of this paper, it will be assumed that the coverage region C of the surveillance system has been determined, the longitude λ_r and conformal latitude ϕ_r of the point of tangency of the master plane have been selected, and the radius E_r of the supporting sphere is given by (28) where k_M and k_m are defined by (24) and (25). The objective of this section is to develop numerical constraints on E_r and other parameters that are to be adhered to in succeeding discussions of the transformation equation.

Let us use ξ_o to denote the angular radius of the smallest circular region with center (ϕ_r, λ_r) that contains F(C) as a subset; i.e.,

$$\xi_o = \min \{\xi : F(C) \subset \bar{X}(\xi)\} \tag{35}$$

As illustrated in Figure 7, ξ_o is the angle at the center of the supporting sphere formed by the radial line through the origin of the w-plane and that passing through the image under the mapping G_r^{-1} of a point of M(C) with modulus ρ satisfying the relation

$$\rho = \max \{|w| : w \in M(C)\} \tag{36}$$

In other words, ρ is the greatest distance separating the point of tangency of the master plane from a point in the image of the coverage region under the mapping M. In this sense, it can be viewed as the maximum modulus of M(C). The focal point for stereographic projection of the supporting sphere onto the master plane lies on the spherical surface diametrically opposite to the point of tangency. Since $\xi_o/2$ is the angle at this point formed by the line through the point of tangency and a line through any point in the master plane removed a distance ρ from it, we conclude that

$$\tan \frac{\xi_o}{2} = \frac{\rho}{2E_r} \tag{37}$$

24

As indicated by the observations of the preceding section, the function $k(\phi,\lambda)$ is the product of $h(\phi)$ and $g(\phi,\lambda)$, defined by (21) and (22), $h(\phi)$ is bounded below by 1 and above by 1.0034, and

$$\max_{(\phi,\lambda)\epsilon F(C)} g(\phi,\lambda) \leq \frac{2}{1+\cos\xi_o} \tag{38}$$

$$\min_{(\phi,\lambda)\epsilon F(C)} g(\phi,\lambda) \geq 1. \tag{39}$$

Consequently,

$$1 \leq k_m \leq k_M \leq \frac{2.0068}{1+\cos\xi_o} \tag{40}$$

and, using (28), we conclude that

$$\frac{a(1+\cos\xi_o)}{2.0068} \leq \frac{a}{k_M} \leq E_r \leq \frac{a}{k_m} \leq a \tag{41}$$

Clearly, the left side of this inequality takes on values between a/2.0068 and a/1.0034 so long as ξ_o is less than 90°. In practice, ξ_o is much less than 90°.

In view of (37) and (41), the minimax radius E_r must satisfy the inequality

$$E \geq \frac{a(1+\cos[2 \text{ arc tan } (\frac{\rho}{2E})])}{2.0068} \tag{42}$$

Suppose now that ρ is a constant less than a/1.0034. Then, as shown in Figure 8, the graph of the right side of the inequality is a monotonic increasing function that approaches a/1.0034 as E increases indefinitely. When E equals $\rho/2$, it assumes the value a/2.0068. Moreover, it is convex down in the range where E exceeds $\rho/2$. Hence, it must intersect the graph of

25

the left side of the inequality above a/2.0068 at some unique value E_o. Consequently, E_o is a lower bound on E_r corresponding to the maximum modulus ρ of $M(C)$ so long as the latter is less than a/1.0034. The relationship between this bound and ρ is illustrated in Figure 9.

The radius E_s is just the distance from the center of the earth to the point on the reference ellipsoid specified by the longitude and geodetic latitude of the radar. Thus, it cannot exceed the equatorial radius, nor can it be less than the polar radius. The minimax solution E_r to the magnification problem is upper bounded by the equatorial radius. A lower bound can be determined from Figure 9 if a numerical value is assigned to ρ. In many practical situations, the greatest distance between the image of a point in the coverage region and the origin of the w-plane is less than 1,000 nautical miles (1 nautical mile = 1,852 meters). Consequently, we will restrict ourselves to the case where ρ does not exceed 1,000 nautical miles.[3] Under this restriction

$$E_r \geq E_o = 6,218,893 \text{ meters} \tag{43}$$

In addition, we shall require the magnitude of w_o, the distance between the w-plane representation of the radar site and the point of tangency, to be no more than 1,000 nautical miles. Finally, the elements of the z-plane represent potential reports of target position from the radar site. Hence, there is little reason to consider points in the z-plane

---

[3] The minimax radius E_r cannot exceed the equatorial radius a. If $F(C)$ can be imbedded in a circular region of angular radius 2 arc tan ($\rho_o/2a$) centered at the master plane point of tangency, then $\rho/2E_r$ is upper bounded by $\rho_o/2a$ and so ρ cannot exceed ρ_o. For example, if $F(C)$ is a subset of a circular region with an angular radius of 16.52°, then ρ cannot exceed 1,000 nautical miles

26

with magnitudes greater than the surveillance range of the radar. We will assume this to be 200 nautical miles.
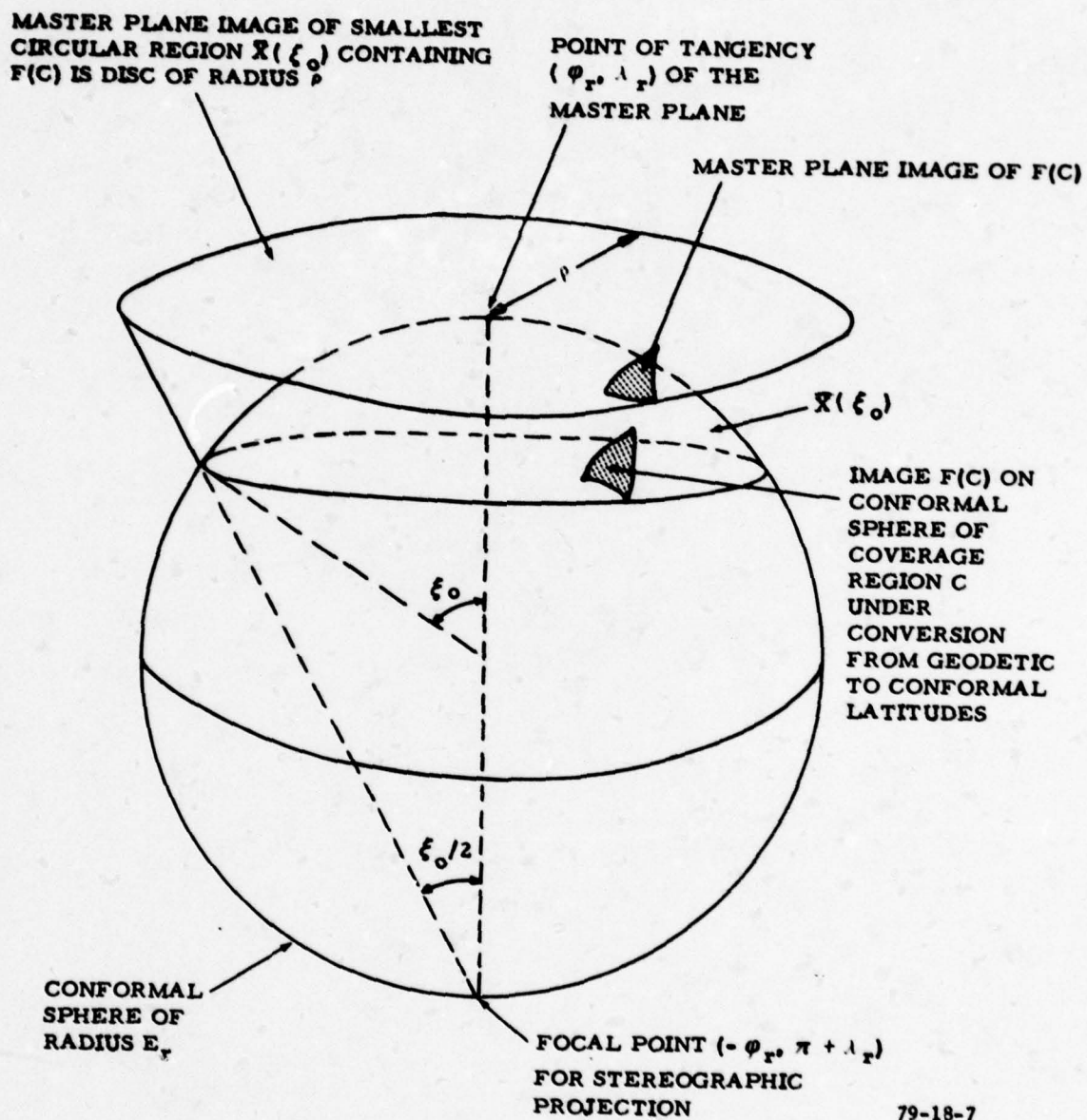
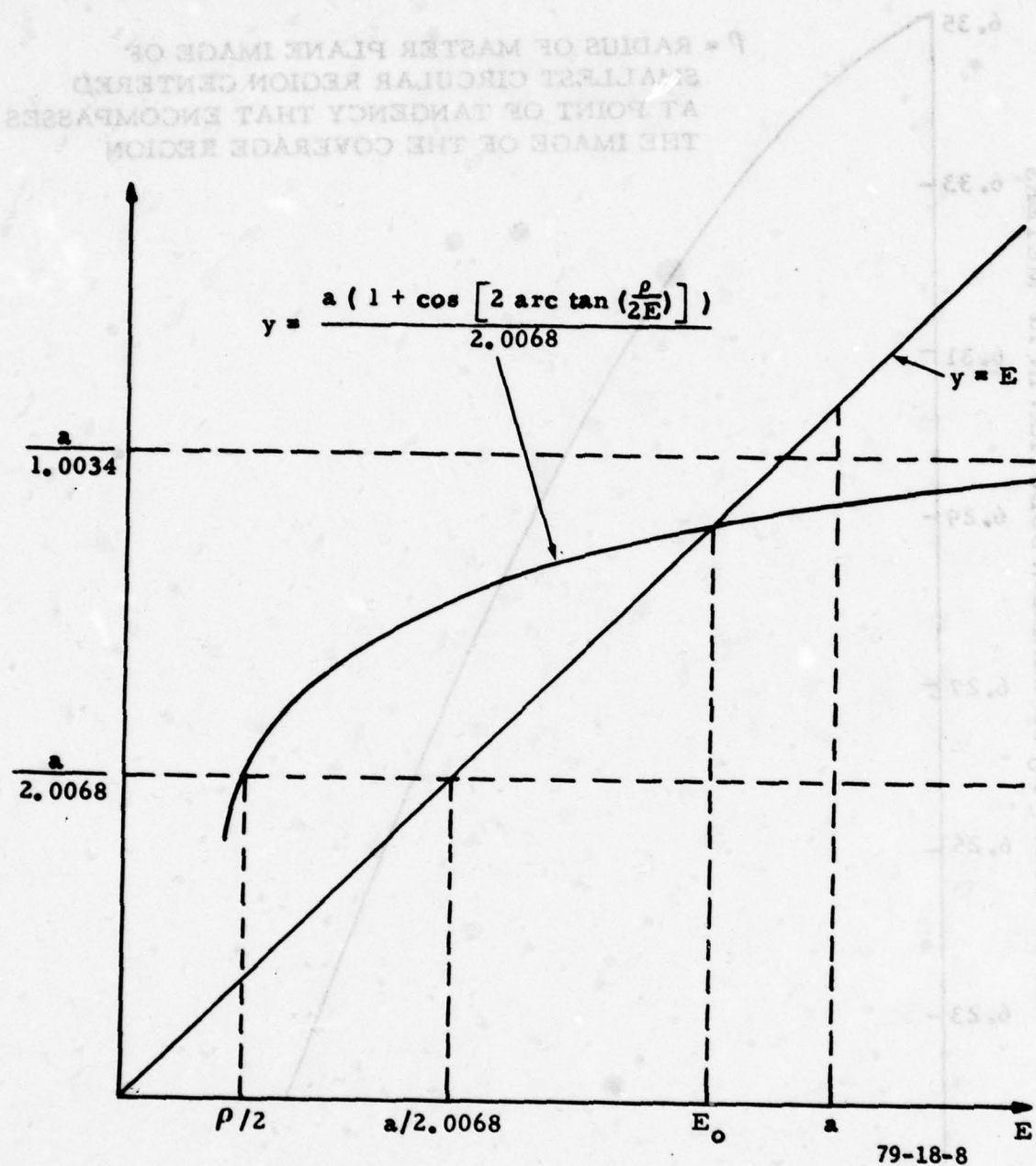FIGURE 7. IMAGES ON THE MASTER PLANE UNDER STEREOGRAPHIC PROJECTION

MASTER PLANE IMAGE OF SMALLEST
CIRCULAR REGION $\mathfrak{X}(\xi_o)$ CONTAINING
F(C) IS DISC OF RADIUS ρ

POINT OF TANGENCY
(φ_r, λ_r) OF THE
MASTER PLANE

MASTER PLANE IMAGE OF F(C)

$\mathfrak{X}(\xi_o)$

IMAGE F(C) ON
CONFORMAL
SPHERE OF
COVERAGE
REGION C
UNDER
CONVERSION
FROM GEODETIC
TO CONFORMAL
LATITUDES

ξ_o

$\xi_o/2$

CONFORMAL
SPHERE OF
RADIUS E_r

FOCAL POINT $(-\varphi_r, \pi + \lambda_r)$
FOR STEREOGRAPHIC
PROJECTION

79-18-7

FIGURE 7.   IMAGES ON THE MASTER PLANE UNDER STEREOGRAPHIC PROJECTION

28

$$y = \frac{a\left(1 + \cos\left[2\ \text{arc tan}\left(\frac{\rho}{2E}\right)\right]\right)}{2.0068}$$

$y = E$

$\frac{a}{1.0034}$

$\frac{a}{2.0068}$

$\rho/2$ a/2.0068 E_O a E

79-18-8

FIGURE 8. DETERMINATION OF LOWER BOUND ON MINIMAX SOLUTION FOR
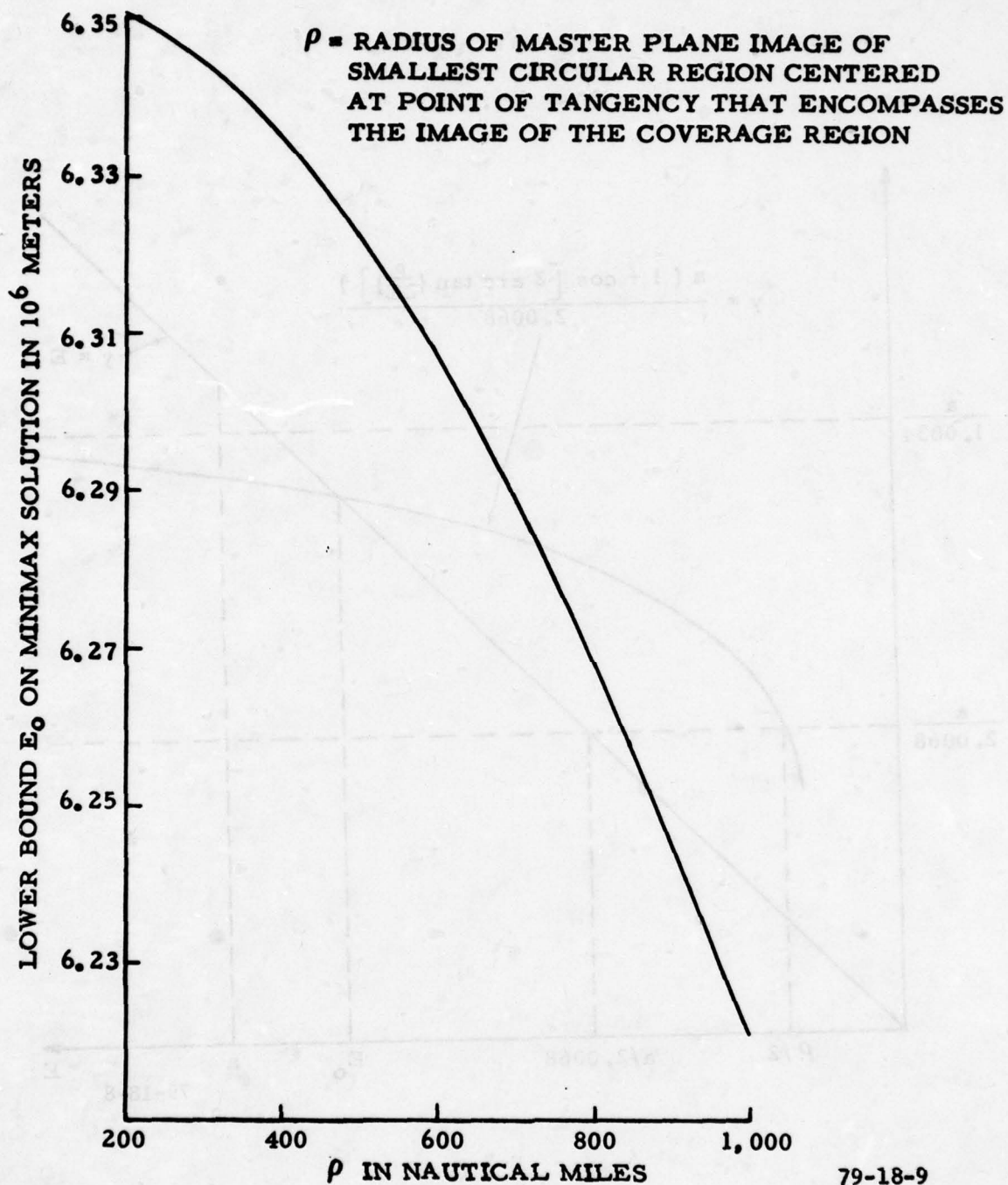RADIUS OF SPHERICAL SUPPORT OF MASTER PLANE

29

FIGURE 9. LOWER BOUNDS ON MINIMAX SOLUTION FOR RADIUS OF SPHERICAL SUPPORT OF MASTER PLANE

8. Polynomial Approximations

The transformation equation (15) can be expressed in the form

$$w = \frac{Az + w_o}{1 - Bw_o^* z} \qquad (44)$$

where

$$A = \frac{E_r}{E_s}\varepsilon^{-i\beta} \quad \text{and} \quad B = \frac{\varepsilon^{-i\beta}}{4E_r E_s}. \qquad (45)$$

Under the constraints imposed in the preceding section, $|Bw_o^* z|$ is always less than 1, and so, using the geometric series, the right side of (44) can be written as the infinite sum

$$w = (Az + w_o)\sum_{k=0}^{\infty}(Bw_o^* z)^k$$

$$= A\sum_{k=0}^{\infty}(Bw_o^*)^k z^{k+1} + w_o + B|w_o|^2\sum_{k=1}^{\infty}(Bw_o^*)^{k-1}z^k$$

$$= w_o + (A + B|w_o|^2)\sum_{k=1}^{\infty}(Bw_o^*)^{k-1}z^k. \qquad (46)$$

Consequently, we will view the image w of z under the transformation equation as the sum of two terms, namely,

$$w = w_n(w_o, z) + e_n(w_o, z)$$

where

$$w_n(w_o, z) = \begin{cases} w_o + (A + B|w_o|^2)\sum_{k=1}^{n}(Bw_o^*)^{k-1}z^k & \text{if } 1 \le n < \infty \\ \\ w & \text{if } n = \infty \quad (47) \end{cases}$$

31

and[4]

$$e_n(w_o, z) = \begin{cases} (A+B|w_o|^2)\sum_{k=n+1}^{\infty}(Bw_o^*)^{k-1}z^k = \dfrac{(A+B|w_o|^2)(Bw_o^*)^n z^{n+1}}{1-Bw_o^* z} & \text{if } 1 \le n < \infty \\[3em] 0 & \text{if } n = \infty \end{cases} \quad (48)$$

In practice, the speed of computational equipment is often insufficient to support an implementation of the transformation equation in its exact form (44). Instead, the equation is approximated by a polynomial of order n in the complex variable z, namely, (47). The difference between the images $w_n(w_o, z)$ and $w_\infty(w_o, z)$ of z under the nth order approximation and the transformation equation itself is given by the complex number $e_n(w_o, z)$. In the following paragraphs, we shall develop upper and lower bounds on the absolute value of this nth order approximation error. Also, we shall examine the increment induced in $w_n(w_o, z)$ by an increment in z. As indicated earlier, it will be assumed that the parameter constraints of the preceding section apply.

---

[4]The parameters E_s and β are determined by the point of tangency (ϕ_r, λ_r) of the master plane and the geodetic coordinates (L_s, λ_s) of the radar site. The inverse of the mapping M defined by (17) carries w_o into (L_s, λ_s). Hence, under the assumption that (ϕ_r, λ_r) and the radius E_r of the spherical support for the master plane are given, the representation of (47) and (48) as functions of w_o and z is appropriate.

9. Transformation Error Bounds

Upper and lower bounds on $|e_n(w_o,z)|$ can be derived from the considerations of Sections 7 and 8. Under the parameter constraints of Section 7, it is clear that

$$\frac{1}{4a}^2 \leq |B| = \frac{1}{4E_r E_s} \leq \frac{1}{4E_o}b \tag{49}$$

$$\frac{E_o}{a} + \frac{|w_o|^2}{4a^2} \leq |A+B|w_o|^2| = \frac{E_r}{E_s} + \frac{|w_o|^2}{4E_r E_s} \leq \frac{a}{b} + \frac{|w_o|^2}{4E_o b} \tag{50}$$

$$\frac{1}{1+\dfrac{|w_o||z|}{4E_o b}} \leq \left| \frac{1}{1-Bw_o^* z} \right| \leq \frac{1}{1-\dfrac{|w_o||z|}{4E_o b}} \tag{51}$$

Moreover, if distance is expressed in nautical miles, then, remembering that $|w_o|$ cannot exceed 1,000 and $|z|$ is upper bounded by 200,

$$\frac{1}{1+\dfrac{|w_o||z|}{4E_o b}} \geq \frac{1}{1+\dfrac{200000}{4E_o b}} \geq .995680 \tag{52}$$

$$\frac{1}{1-\dfrac{|w_o||z|}{4E_o b}} \leq \frac{1}{1-\dfrac{200000}{4E_o b}} \leq 1.00436 \tag{53}$$

Consequently, from (48), we conclude that

$$|e_n(w_o,z)| \leq 1.00436 \left(\frac{a}{b} + \frac{|w_o|^2}{4E_o b} \right) \left(\frac{1}{4E_o}b \right)^n |w_o|^n |z|^{n+1}$$

$$= (1.00776 + 2.17848 \times 10^{-8}|w_o|^2)(2.16902 \times 10^{-8})^n |w_o|^n |z|^{n+1} \tag{54}$$

$$|e_n(w_o,z)| \geq .995680\left(\frac{E_o + |w_o|}{a} + \frac{|w_o|^2}{4a^2}\right) \left(\frac{1}{4a^2}\right)^n |w_o|^n |z|^{n+1}$$

$$= (.970782 + 2.09854 \times 10^{-8}|w_o|^2)(2.10765 \times 10^{-8})^n |w_o|^n |z|^{n+1} \quad (55)$$

The right sides of inequalities (54) and (55) are illustrated in Figures 10 and 11 for the cases where n is 1 and 2. As can be seen from Figure 11, the error in the second order polynomial approximation to the transformation equation is less than 8 meters whenever the distance $|w_o|$ between the origin and the representation of the radar site in the w-plane is less than 1,000 nautical miles, and the representation $|z|$ of the separation between target position and radar in the z-plane does not exceed 200 nautical miles. On the other hand, the error in the first order approximation over the same range of $|z|$ and $|w_o|$ can exceed .8 nautical miles.
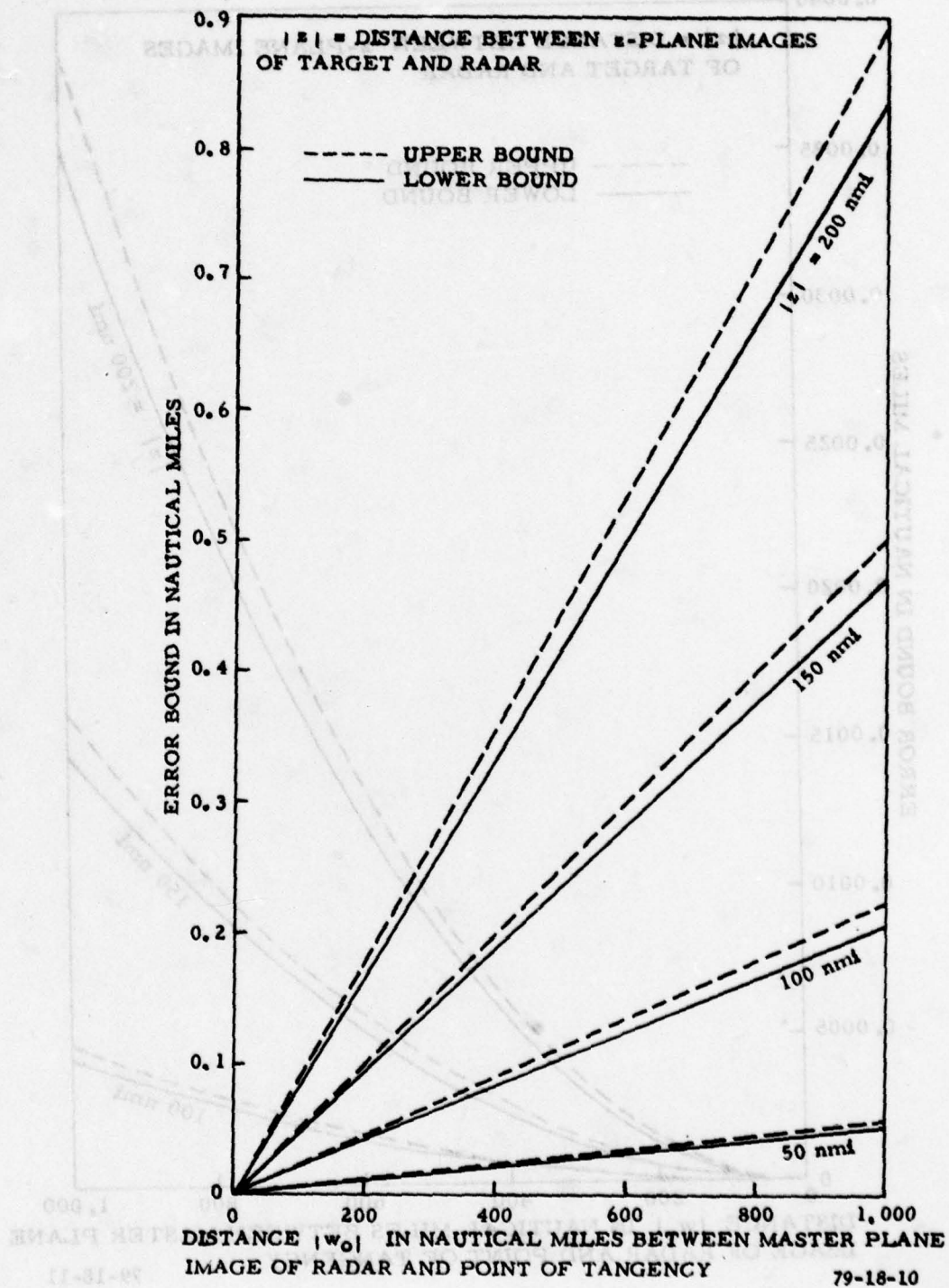
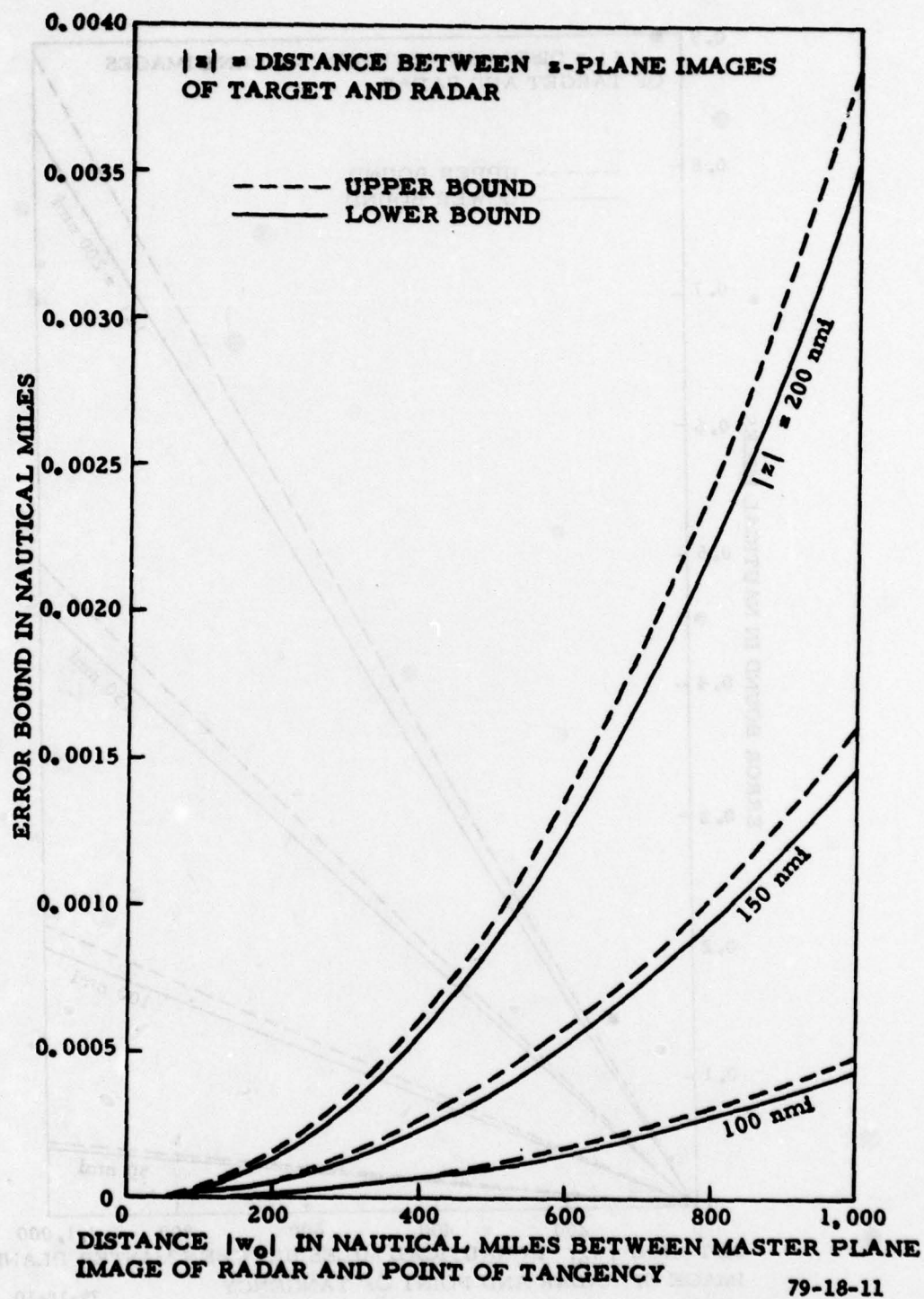FIGURE 10. ERROR BOUNDS FOR THE FIRST-ORDER APPROXIMATION $w_1(w_0, z)$

35

FIGURE 11.   ERROR BOUNDS FOR THE SECOND—ORDER APPROXIMATION $w_2(w_o, z)$

36

10. Increments in Target Location

The z-plane is tangent to a conformal sphere of radius E_s. In this section, the point of tangency will be viewed as the image of the geodetic coordinates (L_s, λ_s) of a radar site under the mapping F defined by (6) and (7). Also, z will be used to denote the z-plane representation of the geodetic coordinates (L, λ) of a target. Thus, z is the image of (L, λ) under the composition $G_s \circ F$ where G_s is defined by (8)-(10). This is not necessarily the same as the z-plane representation of the target in an actual surveillance system. In particular, the method by which the system converts target slant range, azimuth, and altitude into a point in the z-plane may not be equivalent to the mapping $G_s \circ F$. In addition, there are other contributing factors. For example, receiver front-end noise exists, and range, azimuth, and altitude measurements are often quantized before being passed to the central processor. Thus, we can associate two points in the master plane with a single target. One of these is the image of z under the nth order approximation (47) to the transformation mapping. The other is the image of the system z-plane representation $z + \Delta z$ of target location under the same mapping. The difference

$$\Delta w_n = w_n(w_o, z + \Delta z) - w_n(w_o, z) \tag{56}$$

can be treated as the error induced in the master plane by the deviation Δz between correct and apparent z-plane representations of target position. Alternately, Δw_n can be treated as a change induced in master plane representation of position by an increment Δz in the z-plane representing a displacement due to target motion.

In the appendix, it is shown that

$$\Delta w_1 = \epsilon^{-i\beta} \left[\frac{E_r}{E_s} + \left| \frac{w_o}{4E_r E_s} \right|^2 \right] \Delta z \tag{57}$$

Moreover, when n exceeds 1, it is shown that

$$\Delta w_n = \Delta w_1 (1 + \eta_n) \tag{58}$$

where η_n is a function of z, Δz, and w_o. In fact, under the parameter constraints of Section 7,

$$|\eta_n| < .01, \quad 1 < n \leq \infty \tag{59}$$

so long as $|\Delta z|$ does not exceed 10 nautical miles. Thus, as illustrated in Figure 12, Δw_1 accounts for at least 99 percent of the increment Δw_n.

If z is zero, then the function η_n vanishes when Δz goes to zero. Thus, the factor

$$\epsilon^{-i\beta} \left[\frac{E_r}{E_s} + \left| \frac{w_o}{4E_r E_s} \right|^2 \right]$$

is the derivative of w_n with respect to z at the origin of the z-plane. Consequently, a minute displacement from the z-plane origin along the positive portion of the imaginary axis is translated into a displacement from w_o along a directed line segment forming an angle β with the imaginary axis of the w-plane. Thus, as shown in Figure 13, β can be interpreted as the angle between the direction of the North Pole at the point of tangency of the w-plane and the w-plane representation of the northerly direction at the radar site in the z-plane.
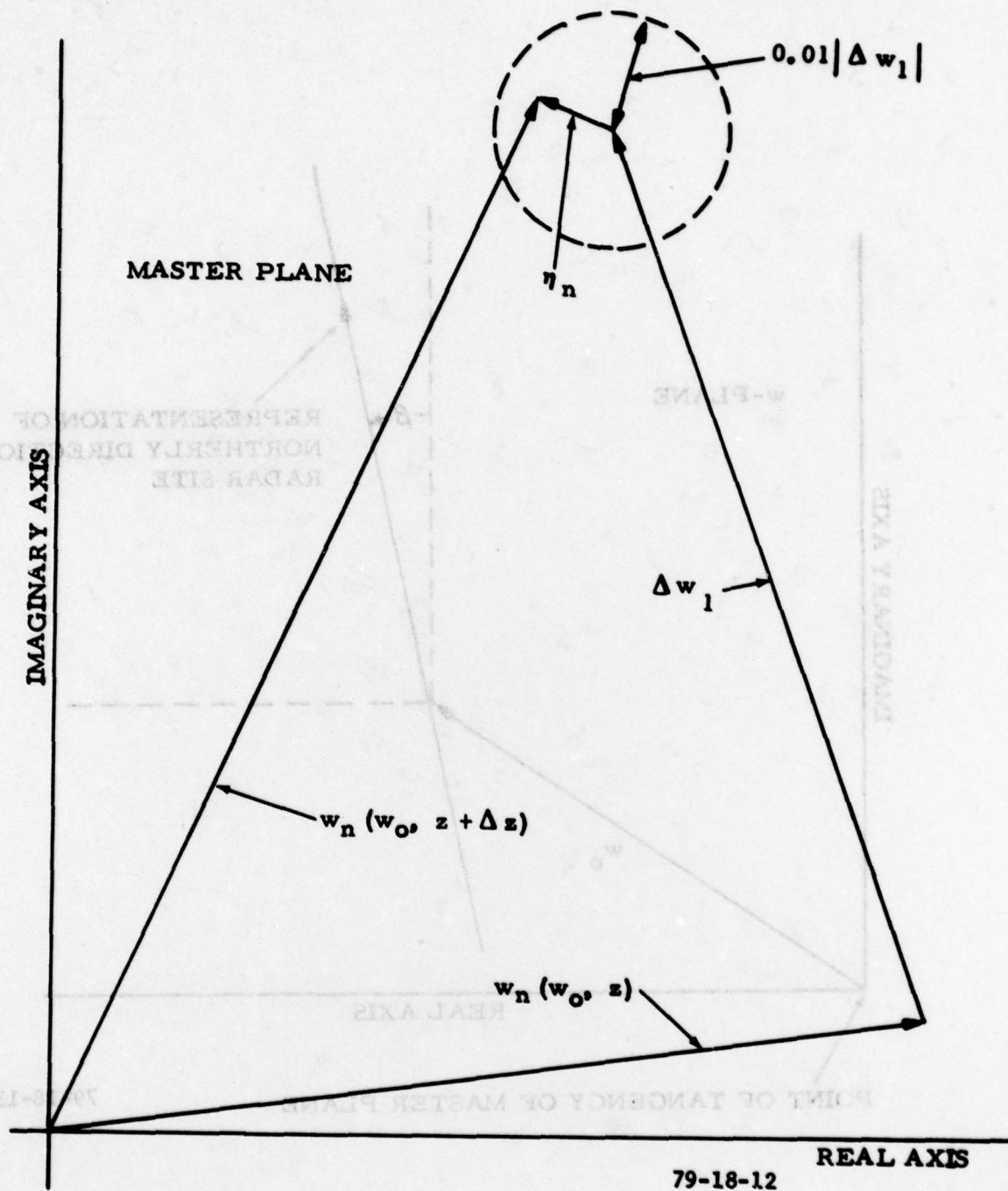
38

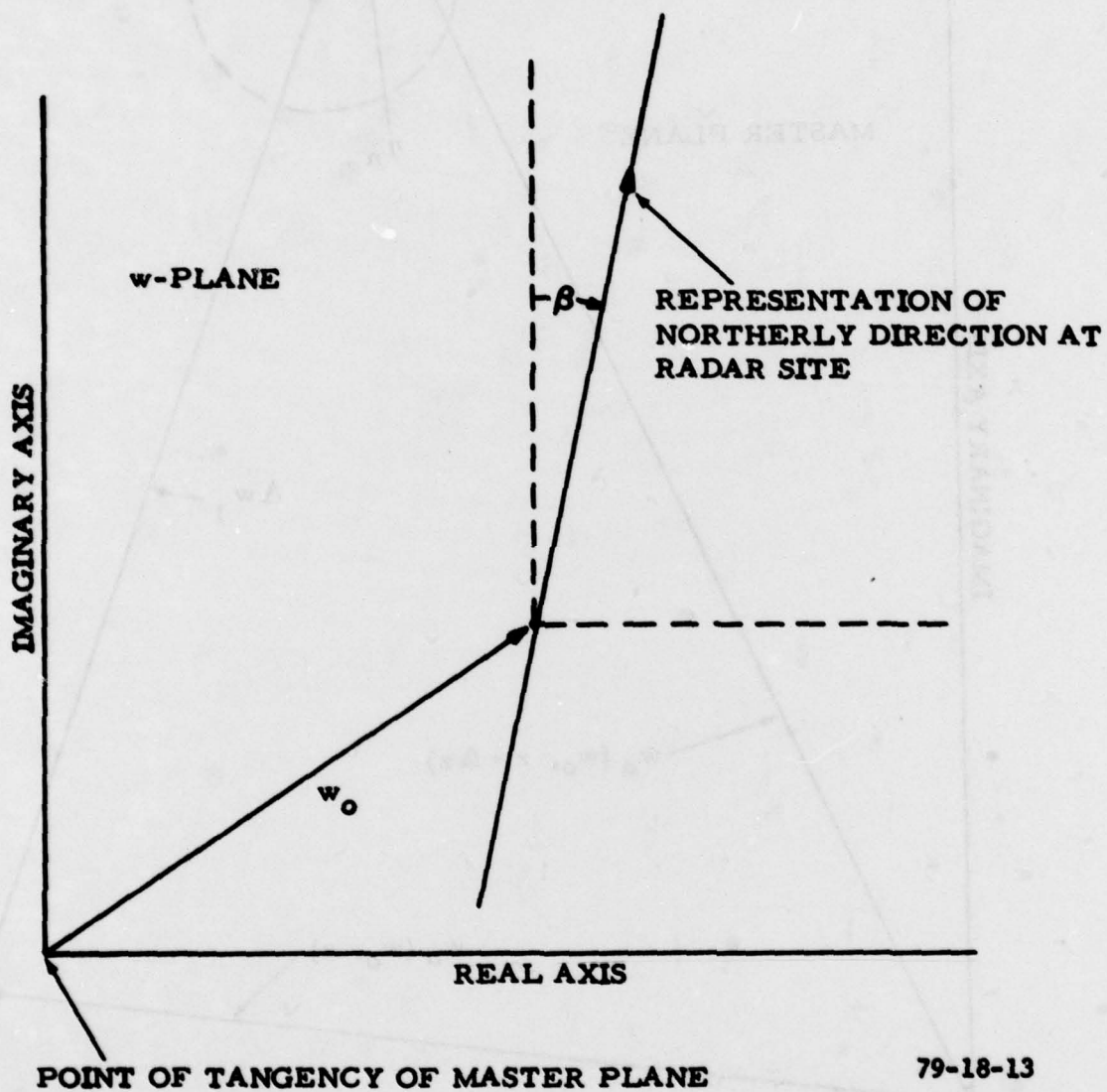FIGURE 12.   EFFECT OF ERROR IN z-PLANE REPRESENTATION OF TARGET LOCATION

FIGURE 13.   ANGLE BETWEEN NORTHERLY DIRECTIONS AT THE RADAR AND THE POINT
OF TANGENCY IN THE MASTER PLANE

40

11. Concluding Remarks

Consideration has been given to master plane magnification of distance on the reference ellipsoid. The magnification factor varies from point to point within the coverage region of the surveillance system. It is also dependent upon the radius of the conformal sphere that supports the master plane. In general, it is possible to choose the radius of the supporting sphere so that the maximum deviation of the magnification factor from unity over the coverage region is minimized.

Determination of the minimax radius is not a difficult task in the case of a circular coverage region. In a strict mathematical sense, such a region is defined in terms of a conformal sphere. However, as a practical matter, it can be thought of as that portion of the reference ellipsoid inside a hollow circular cone with apex at the center of the earth. The intersection of the axis of revolution of the cone with the ellipsoidal surface can be viewed as the center of the region. Likewise, the angle formed at the apex by the intersection of the axis of revolution and any straight line in the conical surface can be regarded as the radius of the region. Roughly speaking, 1 minute of angular radius corresponds to a distance of 1 nautical mile measured along the intersection of the reference ellipsoid and any plane containing the axis of revolution of the cone between the center of the region and its boundary. Thus, a circular region with an angular radius of 10° involves a land mass of approximately 600 nautical miles measured in any direction from the center. In the case of minimax solutions for the radius of the spherical support of the master plane when the circular region is centered at a conformal latitude of 38°, the maximum deviation of the magnification factor from unity

41

increases from .000215 at an angular radius of 2° to .010248 at an angular radius of 16°. Similar results are obtained when the center is moved to other latitudes.

When the coverage region of the surveillance system is not circular, it may be difficult to find the minimax radius for the spherical support of the master plane. Consequently, in some practical situations some sort of suboptimal solution may have to suffice. One possibility is to use the minimax radius associated with a circular region containing the coverage region as a subset. This results in a minimization of the maximum deviation of the magnification factor from unity over the circular region. Moreover, this maximum upper bounds the maximum deviation from unity over the actual coverage region that is generated by the minimax radius associated with the coverage region itself. If the former is very close to 0, then the fact that it is only an upper bound may not be a serious consideration. For example, the center of the circular region might be chosen somewhere near the geographical center of the actual coverage region. Then the angular radius of the circular region can be selected to be just large enough to encompass the entire boundary of the coverage region. In the case where the angular radius is 10° and the center of the circular region is at a conformal latitude of 38°, the upper bound is .004109.

Bounds have been determined for the minimax radius. These can be used in investigations of the transformation process. The equatorial radius of the earth is a trivial upper bound. In addition, there is a lower bound that can be expressed as a monotone decreasing function of an upper limit on the maximum distance between the point at which the master plane is

tangent to its supporting conformal sphere and master plane images of points on the boundary of the coverage region under stereographic projection. For example, the minimax radius is lower bounded by 6,218,893 meters for all coverage regions having a master plane image that is contained inside a circle centered at the point of tangency with a radius of 1,000 nautical miles.

Tight upper and lower bounds have been developed for the absolute difference between master plane images of target location in the local radar plane under the ideal transformation equation and the nth order polynomial approximation thereof. The bounds are based upon three suppositions. First, the radius of the spherical support of the master plane cannot exceed the equatorial radius of the earth, nor can it be less than 6,218,893 meters, the lower bound on the minimax radius for coverage regions having a master plane image contained in a circle with a radius of 1,000 nautical miles centered at the point of tangency. Second, the master plane image of the radar site under stereographic projection must be within 1,000 nautical miles of the point of tangency. Third, the distance between the representation of a target and the representation of the radar on the local radar plane cannot exceed 200 nautical miles.

The first requirement can be met by any coverage region that can be imbedded in a circular region with an angular radius of 16.52°. The radius of the supporting sphere need only be the minimax radius for the coverage region. Alternately, it can be the minimax radius for a circular region with an angular radius of 16.52° or less that encompasses the coverage region. The second condition is insured if the first condition is met and the radar site is located within

43

the coverage region. Obviously, it is also possible to satisfy the second condition in cases where the radar site is outside the coverage region. The third requirement does not impose a serious restriction upon application of the bounds unless the effective range of the radar exceeds 200 nautical miles.

Subject to the three restrictions cited above, a simple relationship has been established between an increment of 10 nautical miles or less in target position in the local radar plane and 99 percent of the corresponding increment induced in the master plane under the nth order approximation to the transformation equation. In general, the increment is essentially multiplied by the value of the derivative of the approximation with respect to target location at the origin of the radar plane. The multiplicative factor depends upon the distance in the master plane between the representation of the radar site and the point of tangency, the radius of the supporting sphere for the master plane, and the distance between the center of the earth and the point on the reference ellipsoid specified by the geodetic coordinates of the radar site. The magnitude of the factor is close to 1. The argument can be interpreted as the master plane representation of the angular deviation between the direction of North at the point of tangency and the direction of North at the radar site.

As a final remark, we emphasize that this investigation does not take into account some basic aspects of practical implementations of the transformation process. These include the use of finite precision arithmetic and various approximations of trigonometric and other mathematical relationships. Such factors can seriously affect the behavior of a surveillance system. To this extent, the results of this paper should be

44

viewed as representative of the transformation process under ideal operating conditions.

<u>REFERENCES</u>

[1] D. Goldenberg and E. Wolf, "A Common Coordinate System
     for the Utilization of Data from Several Radars,"
     Lincoln Laboratory, Lexington, Mass., Technical Report
     No. 67, September 1954.

[2] E. Wolf, "A Stereographic Coordinate System for the
     Utilization of Data from Several Radars," The MITRE
     Corporation, Bedford, Mass., Report No. SR-2, March 1959.

[3] E. Gingerich, "Stereographic Projections in Air Traffic
     Control Systems," <u>Journal</u> <u>of</u> <u>the</u> <u>Institute</u> <u>of</u> <u>Navigation</u>,
     Volume 24, No. 2, Summer 1977.

[4] B. Flax, "Coordinate Conversion and Coordinate Trans-
     formation in the National Airspace System," Institute
     of Transportation and Traffic Engineering, University
     of California, Berkley, California, Report submitted in
     fulfillment of Course CE-299, August 1975.

[5] W. Tveitan, "An Introduction to the Radar Data Collection
     Coordinate Processing and Display Functions in SAGE,"
     The MITRE Corporation, Bedford, Mass., Working Paper
     W-3648 (Appendix A), April 1961.

[6] R. Mulholland and D. Stout, "Numerical Studies of Con-
     version and Transformation in a Surveillance System
     Employing a Multitude of Radars - Part I," National
     Aviation Facilities Experimental Center, Atlantic City,
     N. J., September 1978.

[7] M. Abramowitz and I. Stegun, <u>Handbook</u> <u>of</u> <u>Mathematical</u>
     <u>Functions</u>, National Bureau of Standards, Washington, D. C.,
     1966.

[8] J. Neilson, "Error Minimization in the Stereographic
     Projection," System Development Corporation, Santa Monica,
     Calif., Field Note FN-Lx-151, April 1958.

[9] P. Thomas, "Conformal Projections in Geodesy and Cartog-
     raphy," U. S. Dept. of Commerce, Coast and Geodetic
     Survey, Special Publication No. 251, 1964.

APPENDIX

In what follows, we shall use the identity

$$c^{k-1}(x^k-y^k)=(x-y)\sum_{r=0}^{k-1}(cx)^r(cy)^{k-1-r} \tag{A.1}$$

where k represents any positive integer. It can be verified easily by a straightforward expansion of the expression on the right. In addition, we will use the following proposition.

<u>Proposition</u>: If $0\leq u<1$ and n exceeds 1, then

$$\sum_{k=2}^{n}ku^{k-1}=\frac{2u-u^2-u^n(n+1-nu)}{(1-u)^2}\leq\frac{2u-u^2}{(1-u)^2} \tag{A.2}$$

<u>Proof</u>: The inequality is obvious when u vanishes. Hence, we shall only consider the case where it is positive. Let us use $f(n,u)$ to denote the summation on the left. Clearly,

$$f(n,u)\leq\lim_{n\to\infty}f(n,u) \tag{A.3}$$

over the specified range of the variable u. Moreover,

$$f(n,u)=\frac{d}{du}\sum_{k=2}^{n}u^k=\frac{d}{du}\frac{u^2-u^{n+1}}{1-u}=\frac{2u-u^2-g(n,u)}{(1-u)^2} \tag{A.4}$$

where

$$g(n,u)=u^n(n+1-nu). \tag{A.5}$$

Since

$$\log g(n,u)=n\log u+\log(n+1-nu) \tag{A.6}$$

and the slope of $\log(x+1-xu)$ decreases from $1-u$ to 0 as x increases indefinitely, we conclude that

$$\lim_{n\to\infty}g(n,u)=-\infty \tag{A.7}$$

This implies that $g(n,u)$ approaches 0 as n increases indefinitely. Thus,

$$\lim_{n\to\infty} f(n,u) = \frac{2u-u^2}{(1-u)^2} \qquad (A.8)$$

which establishes the proposition.

We now turn to the development of relationships (57) - (59). It follows from expressions (47) and (56) that

$$\Delta w_n = (A+B|w_o|^2) \sum_{k=1}^{n} (Bw_o^*)^{k-1} [(z+\Delta z)^k - z^k] \qquad (A.9)$$

Applying (A.1), this formula can be written as

$$\Delta w_n = (A+B|w_o|^2) \Delta z \sum_{k=1}^{n} \sum_{r=0}^{k-1} [Bw_o^*(z+\Delta z)]^r [Bw_o^* z]^{k-1-r} \qquad (A.10)$$

Thus,

$$\Delta w_1 = (A+B|w_o|^2) \Delta z, \qquad (A.11)$$

which is equivalent to (57). Moreover, η_n of (58) is given by

$$\eta_n = \sum_{k=2}^{n} \sum_{r=0}^{k-1} [Bw_o^*(z+\Delta z)]^r [Bw_o^* z]^{k-1-r} \qquad (A.12)$$

whenever n exceeds 1.

If $|\Delta z|$ does not exceed 10 nautical miles, and we adhere to the constraints imposed on parameters in Section 7, then

$$|Bw_o^*(z+\Delta z)| \leq \frac{|w_o|(|z|+|\Delta z|)}{4E_r E_s} \leq \frac{(1000)(210)}{4E_o b} = 4.55493 \times 10^{-3}. \qquad (A.13)$$

Letting u represent the right side of this inequality, it follows from (A.2) and (A.12) that

$$|\eta_n| \leq \sum_{k=2}^{n} ku^{k-1} = \frac{2u-u^2-u^n(n+1-nu)}{(1-u)^2}$$

$$\leq \frac{2u-u^2}{(1-u)^2} = 9.17248 \times 10^{-3} \qquad (A.14)$$

whenever $1 < n \leq \infty$.

A-2